© 2020. Published by The Company of Biologists Ltd | Development (2020) 147, dev184234. doi:10.1242/dev.184234

RESEARCH ARTICLE

# Precise coordination of cell-ECM adhesion is essential for efficient melanoblast migration during development

**Amanda Haage[1], Kelsey Wagner[2], Wenjun Deng[2], Bhavya Venkatesh[2], Caitlin Mitchell[2], Katharine Goodwin[3], Aaron Bogutz[4], Louis Lefebvre[4], Catherine D. Van Raamsdonk[4] and Guy Tanentzapf[2,*]**

## ABSTRACT

Melanoblasts disperse throughout the skin and populate hair follicles through long-range cell migration. During migration, cells undergo cycles of coordinated attachment and detachment from the extracellular matrix (ECM). Embryonic migration processes that require cell-ECM attachment are dependent on the integrin family of adhesion receptors. Precise regulation of integrin-mediated adhesion is important for many developmental migration events. However, the mechanisms that regulate integrin-mediated adhesion *in vivo* in melanoblasts are not well understood. Here, we show that autoinhibitory regulation of the integrin-associated adapter protein talin coordinates cell-ECM adhesion during melanoblast migration *in vivo*. Specifically, an autoinhibition-defective talin mutant strengthens and stabilizes integrin-based adhesions in melanocytes, which impinges on their ability to migrate. Mice with defective talin autoinhibition exhibit delays in melanoblast migration and pigmentation defects. Our results show that coordinated integrin-mediated cell-ECM attachment is essential for melanoblast migration and that talin autoinhibition is an important mechanism for fine-tuning cell-ECM adhesion during cell migration in development.

**KEY WORDS: Adhesion, Migration, Talin, Integrins, ECM, Transgenic Mice, Melanocyte**

## INTRODUCTION

Cell migration requires precise coordination of cell attachment to the surrounding extracellular matrix (ECM) (Devreotes and Horwitz, 2015). To allow efficient migration, cells must rapidly form new adhesions to the underlying substrate and then, in a carefully timed fashion, disassemble these adhesions. If cells fail to form enough new adhesions, they are unable to exert pulling forces on the matrix to propel the cell forward. Similarly, if they fail to properly disassemble specific adhesions they will remain attached in place and cease moving (Parsons et al., 2010). It is for this reason that, in migrating cells, the activity of integrins, the main adhesion receptors that mediate cell-ECM adhesion in animals, is under extensive regulation through multiple and diverse mechanisms (Huttenlocher and Horwitz, 2011).

[1]Department of Biomedical Sciences, University of North Dakota, 1301 N Columbia Rd, Grand Forks, ND 58202, ND, USA. [2]Department of Cellular and Physiological Sciences, 2350 Health Sciences Mall, University of British Columbia, Vancouver, BC, Canada. [3]Lewis-Sigler Institute for Integrative Genomics, Princeton University, Princeton, NJ 08540, USA. [4]Department of Medical Genetics, 2350 Health Sciences Mall, University of British Columbia, Vancouver, BC, V6T 1Z3, Canada.

*Author for correspondence (tanentz@mail.ubc.ca)

A.H., 0000-0001-6305-440X; K.G., 0000-0002-4823-7491; L.L., 0000-0001-5664-9480; G.T., 0000-0002-2443-233X

**Handling Editor: Thomas Lecuit**
**Received 28 August 2019; Accepted 8 June 2020**

Integrin regulation has been the subject of intense study, which has shown that integrin activity can be regulated by factors working both inside and outside the cell. Outside the cell, integrins interact with ligands that, upon binding, can induce conformational changes to modulate integrin affinity for the ECM, a process known as outside-in activation (Calderwood, 2004; Ginsberg, 2014). Inside the cell, integrins recruit a large multi-protein adhesion complex that connects to the cytoskeleton and also serves to regulate integrin activity. One of the best-characterized intracellular regulators of integrin activity is the large adapter protein, talin (Tln1). Talin binds to integrins directly and helps recruit, establish and maintain the intracellular adhesion complex (Klapholz and Brown, 2017). In addition, by binding integrin through its C-terminal 'head' domain, talin induces a conformational change in integrins that modulates their affinity for ECM ligands, a process known as inside-out activation (Tadokoro et al., 2003). Owing to its central role in establishing the intracellular adhesion complex and controlling integrin activity, talin function is itself tightly regulated (Goult et al., 2009; Klapholz and Brown, 2017). For example, talin can adopt an autoinhibited conformation that exhibits reduced ability to localize to sites of integrin-mediated adhesion and to activate integrins (Ellis et al., 2013; Goult et al., 2009; Haage et al., 2018), as well as reduced ability to associate with vinculin and actin (Dedden et al., 2019). We recently showed in fibroblasts that a mutation that blocked talin autoinhibition (*Tln1*$^{E1770A}$) increased cell-ECM attachment owing to the presence of more mature, stable adhesions and increased inside-out activation of integrins (Haage et al., 2018). Consequently, mice with the autoinhibition-defective talin mutation exhibited delays in wound healing (Haage et al., 2018).

Regulation of integrin-mediated cell-ECM adhesion is essential for tissue morphogenesis during animal development (Jülich et al., 2015; Pines et al., 2011). An important model for the role of cell-ECM adhesion in tissue morphogenesis has been neural crest cell migration (Loganathan et al., 2016; Perris and Perissinotto, 2000). Neural crest cells are specified after gastrulation at the border of the neural plate and the non-neural ectoderm (Bronner, 2012). These cells undergo an epithelial-to-mesenchymal transition, delaminate and embark on an extensive long-range cell migration process that culminates in their differentiation into multiple cell types, including melanocytes (Mayor and Theveneau, 2013). Melanocytes are melanin-producing cells that play varied and important roles in skin development, and protect adult skin and eyes from damage caused by UV radiation (Tsatmali et al., 2002). Melanocytes originate from precursor cells known as melanoblasts that delaminate from the neural crest and migrate from the dorsum to the ventrum. Unlike other neural crest-derived cells, they originate from either the dorso-lateral pathway or the ventro-medial pathway and eventually reach a final destination in the epithelium, eyes, heart or CNS meninges (Adameyko et al., 2009; Hirobe, 2011; Thomas

Development (2020) 147, dev184234. doi:10.1242/dev.184234

and Erickson, 2008). Melanoblasts undergo extensive proliferation while migrating as spindle-shaped cells. Once migration is complete, they differentiate into dendritic melanocytes or reside as melanocyte stem cells in a hair follicle niche called the bulge (Thomas and Erickson, 2008). Defects in mouse melanocyte development result in pigmentation defects that range from near complete albinism to the presence of small white patches of skin or hair, typically on the belly and feet (Li et al., 2011; Lindsay et al., 2011; Ma et al., 2013; Tokuo et al., 2018; Woodham et al., 2017).

Consistent with their highly migratory behavior, melanoblasts express multiple integrin subunits. However, it has been difficult to address the role of integrin-mediated adhesion in melanoblast migration as these multiple integrin subunits can act redundantly (Beauvais-Jouneau et al., 1999; Hara et al., 1994; Scott et al., 1994). Here, we show that the failure to precisely regulate integrin-mediated cell-ECM adhesion in melanoblasts delays their migration and gives rise to pigmentation defects in mice. Mice expressing autoinhibition-defective talin (*Tln1*$^{E1770A}$) exhibited substantially fewer melanocytes in ventral hair follicles compared with wild-type controls as a result of defective cell migration during embryogenesis. Primary melanocytes derived from the mutant mice exhibited increased adhesion to the ECM and larger, more stable focal adhesions (FAs). As a consequence, these talin autoinhibition-defective primary melanocytes display a less migratory phenotype compared with wild-type, which is mirrored by mutant melanoblasts *in vivo*. Finally, functional analysis of α6 integrin confirms a role for integrin-based adhesion in melanoblast migration. These results show that melanoblast migration requires the precise coordination of cell-ECM adhesion to ensure their robust and efficient migration during embryonic development.

## RESULTS

### Talin autoinhibition mutants exhibit pigmentation defects

We previously reported the generation of mice containing a mutation in talin (*Tln1)* that abrogates its ability to undergo autoinhibition (*Tln1*$^{E1770A}$; Haage et al., 2018). The E1770A mutation changes a conserved glutamate residue that is essential for autoinhibition (Goult et al., 2009). We demonstrated that the overall stability and function of TLN1 containing this mutation was not compromised (Haage et al., 2018). *Tln1*$^{E1770A/E1770A}$ mice were viable and fertile and did not exhibit any gross morphological defects; however, they exhibited characteristic pigmentation defects. Specifically, we noted that on the C57BL/6J genetic background, which has a black coat, 79% ($n$=82) of homozygous *Tln1*$^{E1770A/E1770A}$ mutants had ventrally located white patches (Fig. 1A,B). Additional pigmentation defects included less pigmented tail skin, white tail tips and hypo-pigmented feet (Figs 1C-H). As pigment in mouse hair is produced from melanocytes, their distribution was analyzed in *Tln1*$^{E1770A/E1770A}$ mutants. Skin sections from wild-type *Tln1*$^{+/+}$ and *Tln1*$^{E1770A/E1770A}$ mutant mice were stained for the melanocyte marker dopachrome tautomerase (Dct) and the average number of melanocytes per hair follicle was quantified (Fig. 1I,J). This analysis showed that in dorsal skin sections there were similar numbers of melanocytes per hair follicle in the wild-type and the talin autoinhibition mutants (Fig. 1K). In contrast, in ventral skin sections there were, on average, less than a third as many melanocytes per hair follicle (Fig. 1K). This decrease in melanocyte number is unlikely to be due to decreased TLN1 protein in the mutant, as western blot analysis from neural crest cells (the origin of melanocytes) revealed comparable levels (Fig. 1L), and previous qRT-PCR confirmed similar overall talin expression levels in primary mouse embryonic fibroblasts (MEFs) (Haage et al., 2018). Furthermore, skin sections from ventral white patches revealed the complete absence of Dct-positive cells in hair follicles, which was never observed in the wild type ($n$>50 hair follicles) (Fig. 1M,N). These results show that abrogating talin autoinhibition results in a reduction in the number of melanocytes at sites distant from their developmental origin in the neural crest.

### Melanoblast migration is delayed in Talin autoinhibition mutants

The pigmentation defects observed in *Tln1*$^{E1770A/E1770A}$ mutant mice were consistent with defects seen in previously described mutant strains that affect melanoblast migration, including mutations in Rac1 (Li et al., 2011, 1), P-Rex1 (Lindsay et al., 2011), fascin 1 (Fscn1; Ma et al., 2013), Cdc42 (Woodham et al., 2017) and Myo10 (Tokuo et al., 2018). Melanoblast precursors can be detected as early as 9 days post coitum (E9). Between E9 and E12.5 melanoblasts migrate solely within the dermis. By E12.5, some melanoblasts cross the basement membrane separating the epidermis from the dermis to establish epidermal populations. In the trunk, almost all melanoblasts will enter invaginating hair follicles, which begin forming at E16.5 (Mayer, 1973). In the glabrous skin, (the tail, ears, genitals, nose and ventral paws), melanoblasts are found in the sparsely distributed hair follicles, but are also dispersed in the inter-follicular epidermis and the dermis, where they pigment the skin (Jordan and Jackson, 2000).

To analyze melanoblast migration in *Tln1*$^{E1770A/E1770A}$ mutant mice we introduced into this background the transgenic reporter *Dct*::*lacZ* to mark melanoblasts (Fig. 2; Mackenzie et al., 1997). The progression of migration was analyzed as previously described, by sequentially segmenting the skin into equal sized regions from dorsal to ventral and determining the average density of melanocytes in each segment (see Materials and Methods; Li et al., 2011; Ma et al., 2013; Woodham et al., 2017). No differences in the number of discernable *lacZ*-positive melanoblasts were seen between controls and mutants at E11.5 (Fig. 2A-C). However, in E13.5 embryos the average density of *lacZ*-positive melanoblasts was consistently less in all segments in homozygous *Tln1*$^{E1770A/E1770A}$; *Dct::lacZ* embryos (Fig. 2D,E,G). Also at E13.5, although control *Tln1*$^{+/+}$; *Dct::lacZ* embryos showed *lacZ*-positive melanoblasts extending well into the developing limb, in *Tln1*$^{E1770A/E1770A}$; *Dct::lacZ* mutants this was not the case (Fig. 2F). These defects were even more pronounced in later stage E15.5 embryos, with a reduction in the number of *lacZ*-positive melanoblasts in all segments analyzed for homozygous *Tln1*$^{E1770A/E1770A}$; *Dct::lacZ* mutants (Fig. 2H-K). Taken together these data show that talin autoinhibition controls melanoblast dispersion throughout the skin *in vivo*.

### Melanoblasts in talin autoinhibition mutants proliferate normally, but exhibit a less migratory phenotype than wild type *in vivo*

The proper dispersal of melanoblasts in the skin is dependent on two factors: their ability to migrate and their ability to sufficiently expand their population. A key feature of melanocyte development is the enormous increase in melanoblast numbers that takes place as they undergo cell migration. The overall number of melanoblasts increases from about 100 in E10.5 embryos to about 20,000 by E15.5 (Mort et al., 2015). Integrin-mediated adhesion can regulate cell proliferation (Schwartz and Assoian, 2001). We therefore analyzed melanoblast proliferation in wild-type *Tln1*$^{+/+}$ and *Tln1*$^{E1770A/E1770A}$ mutant embryos (see Materials and Methods; Fig. 3). Melanoblasts were identified using a Dct antibody and

Development (2020) 147, dev184234. doi:10.1242/dev.184234

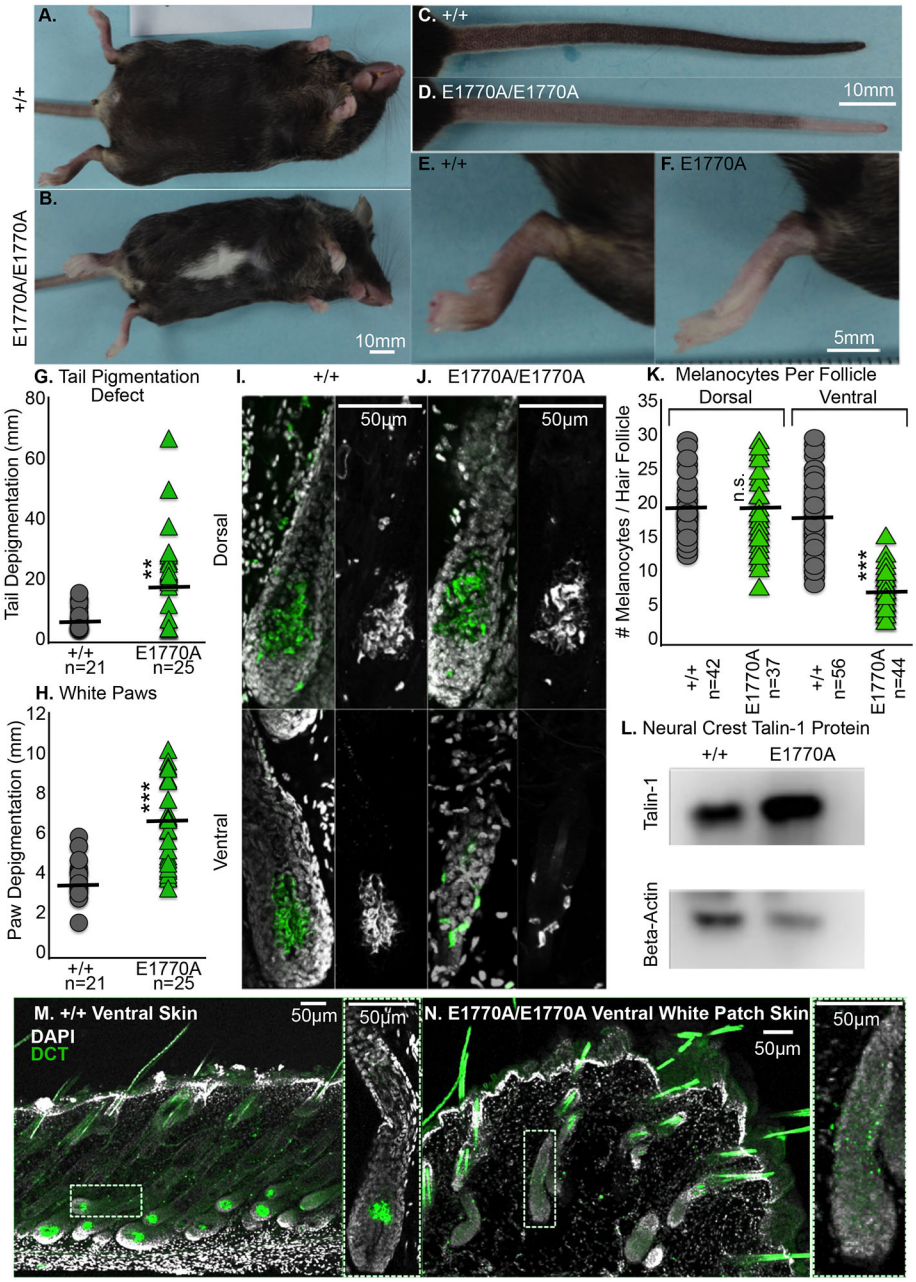


**Fig. 1. Talin autoinhibition mutants exhibit pigmentation defects.** (A,B) Ventral view of adult (A) *Tln1*$^{+/+}$ and (B) *Tln1*$^{E1770A/E1770A}$ male mice at 21 weeks of age. (C-F) Tail (C,D) and rear paw (E,F) of mice presented in A. (G) Length of depigmented bands present on *Tln1*$^{+/+}$ (gray circles) and *Tln1*$^{E1770A/E1770A}$ (green triangles) mice tails; black bar represents mean. (H) Length of white area from toe tip present on *Tln1*$^{+/+}$ (gray circles) and *Tln1*$^{E1770A/E1770A}$ (green triangles) mice paws; black bar represents mean. (I,J) Representative images of single hair follicles from dorsal (top) and ventral (bottom) skin sections stained with DAPI (white) and a Dct antibody (green) from *Tln1*$^{+/+}$ and *Tln1*$^{E1770A/E1770A}$ mice at 4 weeks of age (left panels). Right panels show stains with Dct antibody only (white). (K) Average number (black bar represents mean) of melanocytes per hair follicle in dorsal and ventral skin sections from *Tln1*$^{+/+}$ (gray circles) and *Tln1*$^{E1770A/E1770A}$ (green triangles) mice at 4 weeks of age. *n*-value on graph is number of hair follicles analyzed across >3 mice per genotype. (L) Western blot analysis of neural plates removed from E8.5 *Tln1*$^{+/+}$ and *Tln1*$^{E1770A/E1770A}$ embryos. (M,N) Representative images of multiple hair follicles in a ventral skin sections stained with DAPI (white) and a Dct antibody (green) from 4-week-old mice. Panel on right shows magnification of boxed area on left. ***$P \leq 0.001$, **$P \leq 0.01$ (Student's *t*-test). n.s., not significant.

5-ethynyl-2′-deoxyuridine (EdU) labeling was used to track cell proliferation. E15.5 wild-type *Tln1*$^{+/+}$ and homozygous *Tln1*$^{E1770A/E1770A}$ mutant embryos were harvested and fixed for staining 4 and 24 h post injection of the pregnant female with EdU (Fig. 3A-D). This analysis found similar numbers of Dct and EdU double-positive cells in trunk skin sections at both time points, consistent with the conclusion that modulating talin autoinhibition does not affect melanocyte proliferation (Fig. 3E). In contrast, analysis of the cell shape of melanoblasts in wild-type *Tln1*$^{+/+}$ and *Tln1*$^{E1770A/E1770A}$ mutant embryos revealed changes consistent with alteration in their migratory phenotype (Fig. 3F). First, analysis (see Materials and Methods) of Dct-positive melanoblast shape was performed in the trunk cross sections from E15.5 embryos to measure their area, circularity and aspect ratio. Compared with wild-type *Tln1*$^{+/+}$ controls, Dct-positive melanoblasts from *Tln1*$^{E1770A/E1770A}$ mutant mice were rounder, less elongated and occupied less area, all of which are consistent with a reduced migratory phenotype (Fig. 3G-I). Second, this analysis was repeated in the context of the intact skin by taking high magnification images of *lacZ*-positive melanoblasts from *Dct::lacZ* whole E15.5 embryos (Fig. S1A). Again, analysis of *lacZ*-positive melanoblast shape was performed for embryos from wild-type *Tln1*$^{+/+}$; *Dct::lacZ* and *Tln1*$^{E1770A/E1770A}$; *Dct::lacZ* mutants to measure their area, circularity and aspect ratio. This analysis showed that, even in the context of the intact skin of whole embryos, mutant *lacZ*-positive melanoblasts were slightly rounder and occupied less area, all of which are consistent with a reduced migratory phenotype (Fig. S1B-D).

Integrin-mediated adhesion can also regulate ECM production (Hornberger et al., 2000; Schwartz, 2010). We therefore also analyzed melanoblast association with the basement membrane component collagen IV (Fig. 3J,K). No obvious change in collagen

Development (2020) 147, dev184234. doi:10.1242/dev.184234

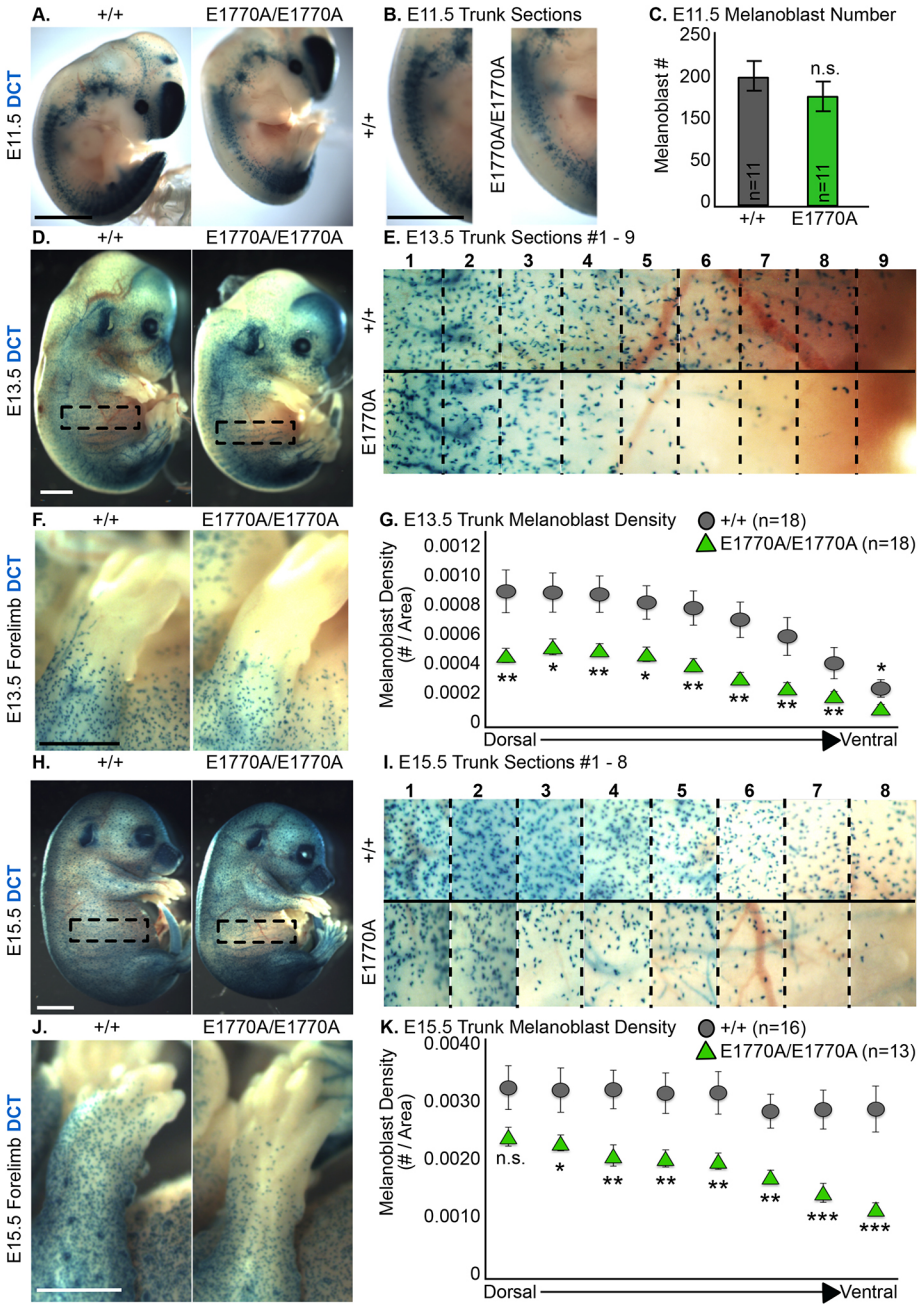


**Fig. 2. Loss of talin autoinhibition delays melanoblast migration.** (A) Representative X-gal-stained E11.5 *Dct::lacZ* embryos of *Tln1*$^{+/+}$ and *Tln1*$^{E1770A/E1770A}$ genotypes. (B) Sections of E11.5 embryos shown in A that were further analyzed and quantified. (C) Average number of melanoblasts counted in the E11.5 segment shown in A. (D,E) Representative X-gal-stained E13.5 *Tln1*$^{+/+}$; *Dct::lacZ* and *Tln1*$^{E1770A/E1770A}$; *Dct::lacZ* embryos. Boxed areas indicate trunk regions, expanded in E, in which melanoblasts were quantified in G. (F) Representative X-gal-stained forelimbs from *Tln1*$^{+/+}$; *Dct::lacZ* and *Tln1*$^{E1770A/E1770A}$; *Dct::lacZ* E13.5 embryos. (G) Average melanoblast density (number/segment area) from the E13.5 embryo trunk segments shown in E. (H) Representative X-gal-stained E15.5 *Tln1*$^{+/+}$; *Dct::lacZ* and *Tln1*$^{E1770A/E1770A}$; *Dct::lacZ* embryos. Boxes indicate the position of quantified trunk regions, expanded in I. (I) Segments of E15.5 embryos in H that were quantified in K. (J) Representative X-gal-stained forelimbs from E15.5 *Tln1*$^{+/+}$; *Dct::lacZ* and *Tln1*$^{E1770A/E1770A}$; *Dct::lacZ* embryos. (K) Average melanoblast density (number/segment area) from E15.5 embryo trunk segments. Error bars denote s.e.m. ***$P \leq 0.001$, **$P \leq 0.01$, *$P \leq 0.05$ (Student's *t*-test). n.s., not significant. Scale bars: 500 µm in A,B; 1 mm in D,F,J; 2 mm in H.

IV was seen in trunk cross sections from E15.5 *Tln1*$^{E1770A/E1770A}$ embryos, and the correlation coefficient between collagen IV and Dct-positive melanoblasts was similar compared with wild-type controls (Fig. 3L). Taken together, these data suggest that the defects in melanoblast dispersal observed in talin autoinhibition mutants are the result of defective cell migration rather than changes in cell proliferation or basement membrane organization.

### Talin autoinhibition regulates cell shape and protrusivity, but not actin organization in primary melanocyte culture

To further investigate the effects of talin autoinhibition, melanocytes were isolated from 3-day-old wild-type *Tln1*$^{+/+}$ or *Tln1*$^{E1770A/E1770A}$ mutant neonatal trunk skin and cultured for 6 weeks as previously described (Fig. 4A; Sviderskaya et al., 1997). Automated image analysis was used to analyze the cell area, circularity and aspect ratio of these cells. Overall, this analysis showed that melanocytes from *Tln1*$^{E1770A/E1770A}$ mutant mice had smaller area, were more round and were less elongated than those from control *Tln1*$^{+/+}$ mice (Fig. 4B-D). Next, cell protrusions were quantified in control and talin autoinhibition-defective melanocytes. Melanocytes from *Tln1*$^{E1770A/E1770A}$ mutant mice had fewer protrusions, but there was no substantial difference in protrusion shape compared with melanocytes from *Tln1*$^{+/+}$ control mice (Fig. 4E,F). As changes in cell shape and a reduction in cell protrusions can be associated with altered actin architecture, two quantitative approaches were used to analyze the actin cytoskeleton in these melanocytes (Fig. 4G,H). First, we measured the overall level of actin alignment in a cell (see Materials and Methods; Cetera et al., 2014; Haage et al., 2018). No substantial differences were observed in actin alignment between *Tln1*$^{E1770A/E1770A}$ mutant or *Tln1*$^{+/+}$ control melanocytes (Fig. 4I). Next, the percentage of the cell that contains aligned bundles, termed cell fibrousness, was

Development (2020) 147, dev184234. doi:10.1242/dev.184234

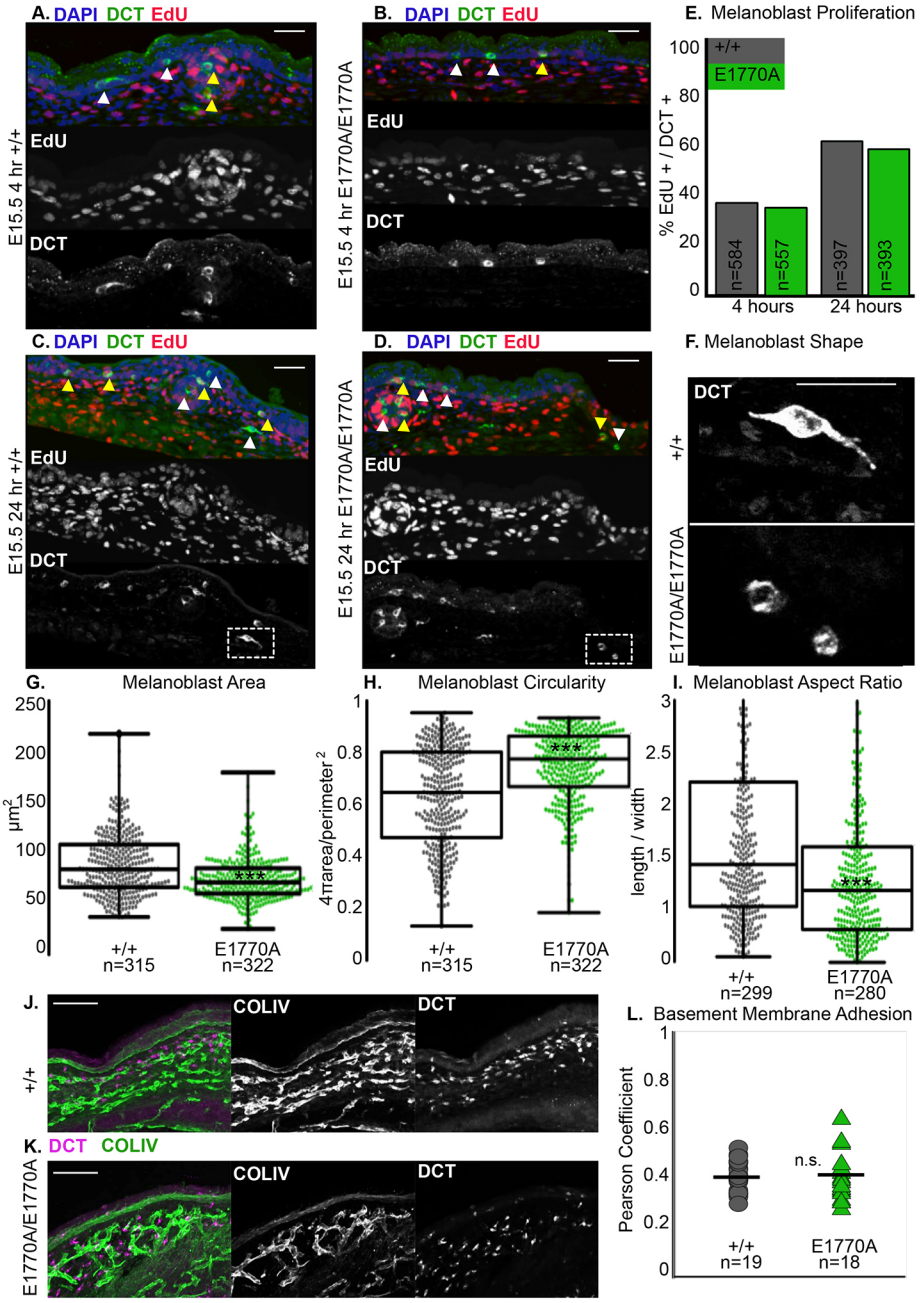


**Fig. 3. Melanoblasts in talin autoinhibition mutants proliferate normally, but exhibit changes in cell shape.** (A,B) Representative images of transverse sections of E15.5 *Tln1*$^{+/+}$ (A) and *Tln1*$^{E1770A/E1770A}$ (B) embryonic skin stained with DAPI (blue), Dct (green) and EdU (red). Embryos were harvested 4 h post EdU injection. (C,D) Representative images of transverse sections of E15.5 *Tln1*$^{+/+}$ (C) and *Tln1*$^{E1770A/E1770A}$ (D) embryo skin stained with DAPI (blue), Dct (green) and EdU (red). Embryos were harvested 24 h post EdU injection. White arrowheads indicate Dct-positive melanoblasts without EdU; yellow arrowheads indicate Dct-positive melanoblasts with EdU. (E) Mean number of cells found positive for both Dct and EdU in three embryos per genotype, harvested at 4 h or 24 h post EdU injection. (F) Magnification of boxed areas in C and D showing melanoblasts stained with Dct. (G) Melanoblast areas from Dct-positive cells in transverse sections across three embryos per genotype harvested 24 h post EdU injection. (H) Melanoblast circularity, defined as 4π area/perimeter$^2$, from Dct-positive cells in transverse sections across three embryos per genotype, harvested 24 h post EdU injection. (I) Melanoblast aspect ratios from Dct-positive cells in transverse sections across three embryos per genotype, harvested 24 h post EdU injection. Outlying data points above an aspect ratio of three were excluded. (J,K) Representative images of transverse sections of E15.5 *Tln1*$^{+/+}$ (J) and *Tln1*$^{E1770A/E1770A}$ (K) embryonic skin stained for collagen IV (COLIV; green) and Dct (magenta). (L) Pearson's correlation coefficient between collagen IV and Dct staining in transverse sections of E15.5 embryos. *n*-value is the number of sections analyzed in three embryos per genotype; black bar represents mean. Box plots show minimum/maximum whiskers with box boundaries as Q1/Q3 and center line representing the median. ***$P \leq 0.001$ (Student's *t*-test). n.s., not significant. Scale bars: 50 µm in A-D,F; 100 µm in J,K.

measured (see Materials and Methods; Haage et al., 2018), and again no substantial differences were observed between melanocytes from either *Tln1*$^{E1770A/E1770A}$ mutant mice or *Tln1*$^{+/+}$ controls (Fig. 4J). Taken together, our data show that cell shape is altered in talin autoinhibition-defective mutants, but that these phenotypes cannot be explained simply by changes in actin organization.

### Talin autoinhibition regulates focal adhesion maturation in melanocytes

To investigate how talin autoinhibition results in altered cell shape and defective cell migration, FAs, which mediate attachment to the ECM during cell migration (Wozniak et al., 2004), were analyzed in detail in melanocytes. To investigate the effect of the E1770A mutation on FAs, primary melanocytes from 3-day-old *Tln1*$^{+/+}$ or *Tln1*$^{E1770A/E1770A}$ mutant neonatal mice were isolated and cultured. FA number, composition and shape were determined in wild-type and mutant melanocytes using multiple markers in combination with high resolution quantitative automated image analysis (see Materials and Methods; Fig. 5). In melanocytes from either *Tln1*$^{+/+}$ controls or *Tln1*$^{E1770A/E1770A}$ mutants characteristic FAs and stress fibers were present (Fig. 5A). However, there was an ∼25% reduction in the number of FAs in melanocytes from *Tln1*$^{E1770A/E1770A}$ mutant mice compared with those from control *Tln1*$^{+/+}$ mice (Fig. 5B). Moreover, there was an increase of 15% and 10%, respectively, in FA area and aspect ratio of melanocytes from *Tln1*$^{E1770A/E1770A}$ mutant mice compared with those from control *Tln1*$^{+/+}$ mice (Fig. 5C,D). Importantly, plotting histograms showing the distribution of FA areas in melanocytes from *Tln1*$^{E1770A/E1770A}$ mutants or control *Tln1*$^{+/+}$ mice revealed an increase in the percent of FAs over 1 µm$^2$ in size (Fig. 5E). A characteristic of maturing adhesions is that as they increase in area they also elongate (Geiger and Yamada, 2011;

Development (2020) 147, dev184234. doi:10.1242/dev.184234

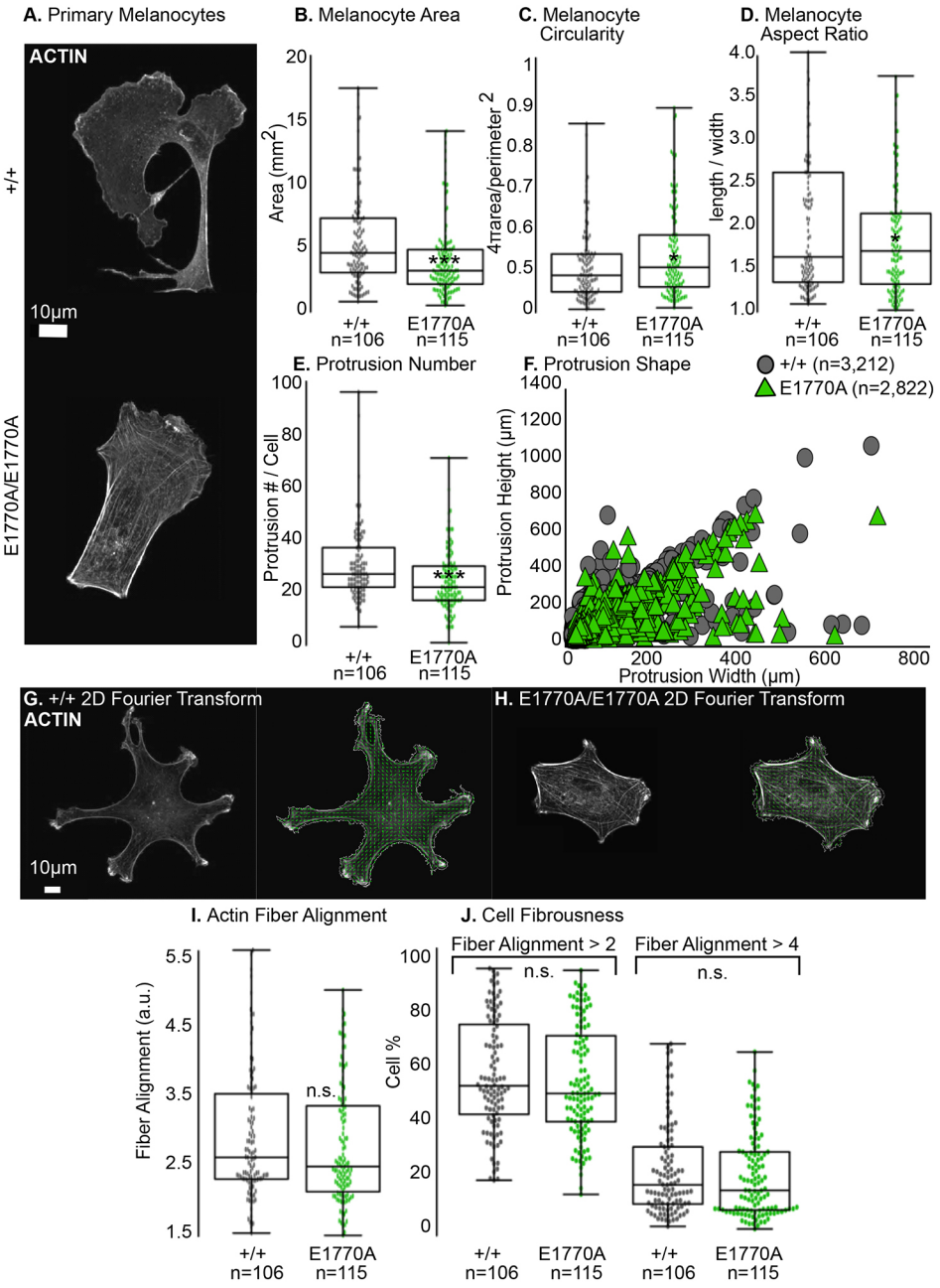


**Fig. 4. Talin autoinhibition regulates primary melanocyte cell shape.** (A) Representative images of primary melanocytes with actin stained by phalloidin (white). (B) Primary melanocyte areas. (C) Primary melanocyte circularities. (D) Primary melanocyte aspect ratios. (E) Average number of actin-based protrusions per cell. (F) Protrusion shape described as protrusion height in μm (*y*-axis) over protrusion width in μm (*x*-axis). *n*-values are individual protrusions over the number of cells indicated in B-E. (G,H) Representative images of $Tln1^{+/+}$ (G) and $Tln1^{E1770A/E1770A}$ (H) primary melanocytes plated on fibronectin for 180 min, with actin stained by phalloidin (white). On the right, the image was overlaid with the 2D Fourier transform analysis (see Materials and Methods). (I) Actin fiber alignment of phalloidin-stained primary melanocytes plated on fibronectin. (J) Cell fibrousness, defined as the percentage of the cell with an actin fiber alignment above a strict (>4) or relaxed (>2) cutoff. Box plots show minimum/maximum whiskers with box boundaries as Q1/Q3 and center line representing the median. ***$P \leq 0.001$, *$P \leq 0.05$ (Student's *t*-test). n.s., not significant.

Wolfenson et al., 2009). We determined that the average aspect ratio of FAs was consistently larger in melanocytes from $Tln1^{E1770A/E1770A}$ mutants when compared with melanocytes from control $Tln1^{+/+}$ mice irrespective of FA area (Fig. 5F). These measurements reveal that the $Tln1^{E1770A}$ mutation increased the number of larger, more elongated adhesions in melanocytes, consistent with an overall increase in FA maturation.

Increased maturation of FAs is correlated with increased integrin activation and adhesion (Haage et al., 2018; Lee et al., 2013). To test whether the $Tln1^{E1770A}$ mutation promoted integrin activation, we used the active β1-integrin-specific antibody 9EG7 (Bazzoni et al., 1995). Melanocytes from control $Tln1^{+/+}$ or $Tln1^{E1770A/E1770A}$ mice were co-stained using a general β1-integrin antibody and 9EG7. The ratio of staining intensity of these two antibodies within FAs was used to measure activation. These data showed an increase in integrin activation in melanocytes from $Tln1^{E1770A/E1770A}$ mice (Fig. 5G,H). In addition, increased FA maturation and higher integrin activation seen in melanocytes from $Tln1^{E1770A/E1770A}$ mutants would be expected to change the strength of cell-ECM adhesions. To directly address this point, we used an assay that employs a coverslip-spinning device to measure the strength of cell-ECM attachment in wild-type and mutant melanocytes (see Materials and Methods; García et al., 1997; Haage et al., 2018). In this assay the relative attachment strength of cells to an underlying ECM is measured by first incubating them on fibronectin-coated coverslips so that they can attach, and then spinning the coverslips, creating centrifugal forces that detach more loosely affixed cells. Relative adhesion strength is calculated by determining the ratio of cells attached after spinning compared with a same-day non-spun control. This technique revealed that melanocytes derived from $Tln1^{E1770A/E1770A}$ mice showed stronger attachment to the ECM relative to melanocytes derived from control

Development (2020) 147, dev184234. doi:10.1242/dev.184234

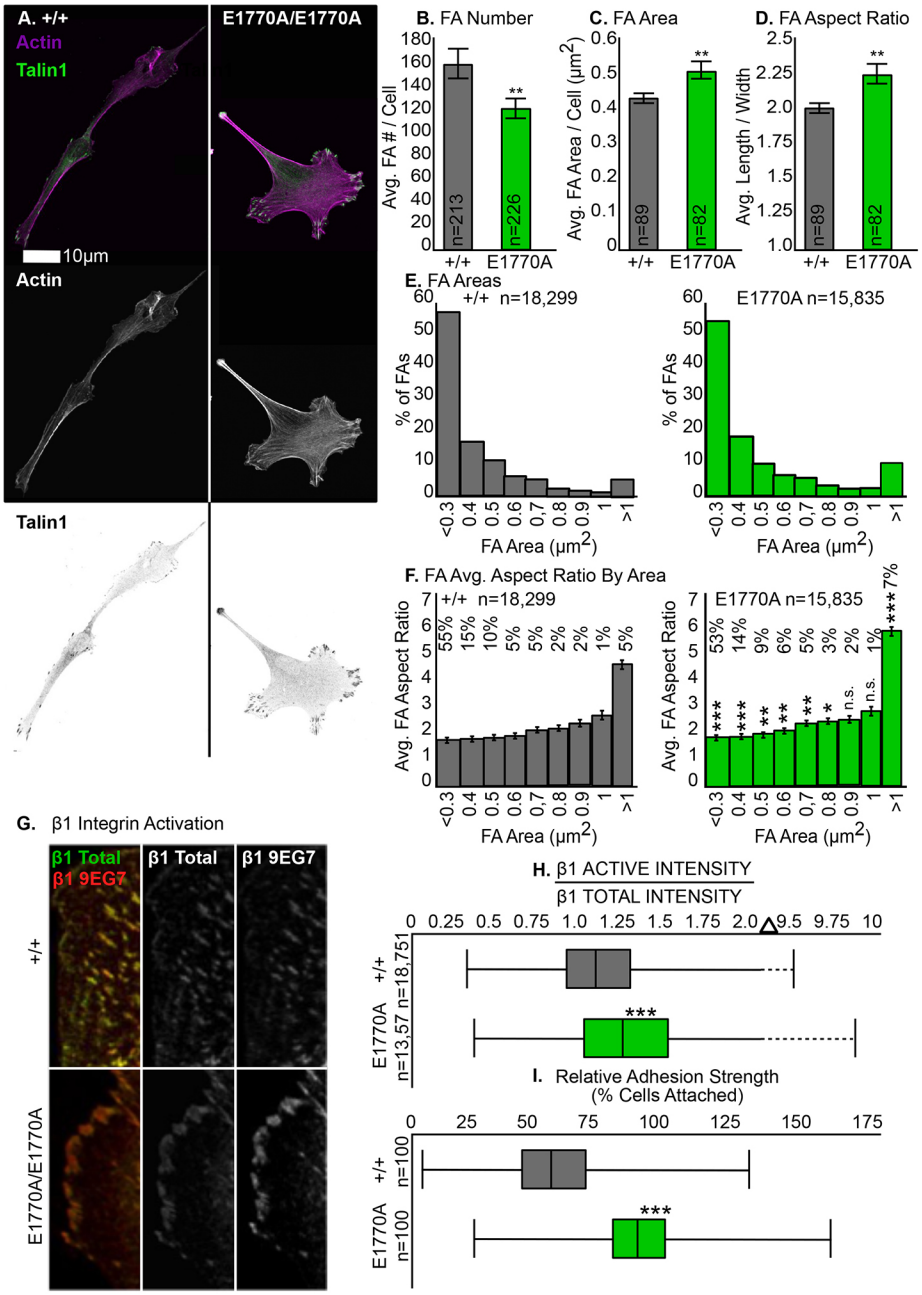


**Fig. 5. Talin autoinhibition regulates FA maturity in primary melanocytes.** (A) Representative images of primary melanocytes with actin stained by phalloidin (magenta, top; white, middle) and FAs stained by talin 1 (green, top; black, bottom). (B) Mean number of FAs per primary melanocyte. (C) Average FA area per primary melanocyte. (D) Average FA aspect ratio per primary melanocyte. (E) FA areas binned in groups ranging from <0.3 μm$^2$ to >1 μm$^2$ for each genotype. *n*-values represent individual FAs. (F) Mean FA aspect ratio for each binned group of FA areas per genotype. *n*-values represent percentage of total individual FAs (reported in E) per bin. (G) Representative images of 3.5 μm of the leading edge of primary melanocytes plated on fibronectin for 180 min and stained with the active β1-integrin-specific monoclonal antibody 9EG7 (red) and a polyclonal β1-integrin antibody (green). (H) Ratio of FA intensities from the staining of active β1-integrin to total β1-integrin, on the date represented in G. *n*-values represent individual FAs. (I) Cell counts for cell-spinning assay per genotype. *n*-values represent numbers of cells. Box plots show minimum/maximum whiskers with box boundaries as Q1/Q3 and center line representing the median. Error bars denote s.e.m. ***$P \leq 0.001$, **$P \leq 0.01$, *$P \leq 0.05$ (Student's *t*-test). n.s., not significant.

*Tln1*$^{+/+}$ mice (Fig. 5I). In summary, these findings suggest that there are fewer FAs in melanocytes derived from *Tln1*$^{E1770A/E1770A}$ mice, but that these FAs are on average bigger, more mature, contain more activated integrin and mediate stronger attachment to the underlying ECM.

### Talin autoinhibition regulates migration speed and persistence in melanoblasts

The changes in morphology, FA number and shape, and cell-ECM adhesion observed in primary melanocytes from *Tln1*$^{E1770A/E1770A}$ mice predicts altered melanoblast migration throughout development. To directly analyze melanoblast migration in their natural environment, the intact epidermis, segments of E15.5 embryonic trunk skin were isolated, cultured and imaged *ex vivo* (Fig. 6; Movies 1-4). These explants were cultured as previously described (see Materials and Methods; Cetera et al., 2018; Mort et al., 2015) and imaged for 4 h. To visualize melanoblasts, the melanocyte-specific *Mitf-cre* transgene was used to induce Tomato expression from a *Rosa26-floxed stop-TdTomato* ('Rosa26-Tom') fluorescent reporter (Alizadeh et al., 2008; Madisen et al., 2010). This labeled all embryonic melanoblasts (Huang et al., 2015) and was introduced into wild-type and mutant backgrounds (Fig. 6A; Movies 1-4). Importantly, melanoblasts in talin autoinhibition-defective explants exhibited smaller area, greater circularity and lower aspect ratio compared with melanoblasts from wild-type controls (Fig. 6C-E, left). These results were in line with our observation from primary melanocytes (Fig. 4A-C) and fixed and *lacZ*-labeled melanoblasts in the context of intact mouse skin. (Fig. S1). Using the open source ImageJ plugin ADAPT for automated tracking of individual migrating cells (Fig. 6B; Barry et al., 2015) we observed reduced dynamics and an altered migratory phenotype in melanoblasts lacking talin autoinhibition.

Development (2020) 147, dev184234. doi:10.1242/dev.184234

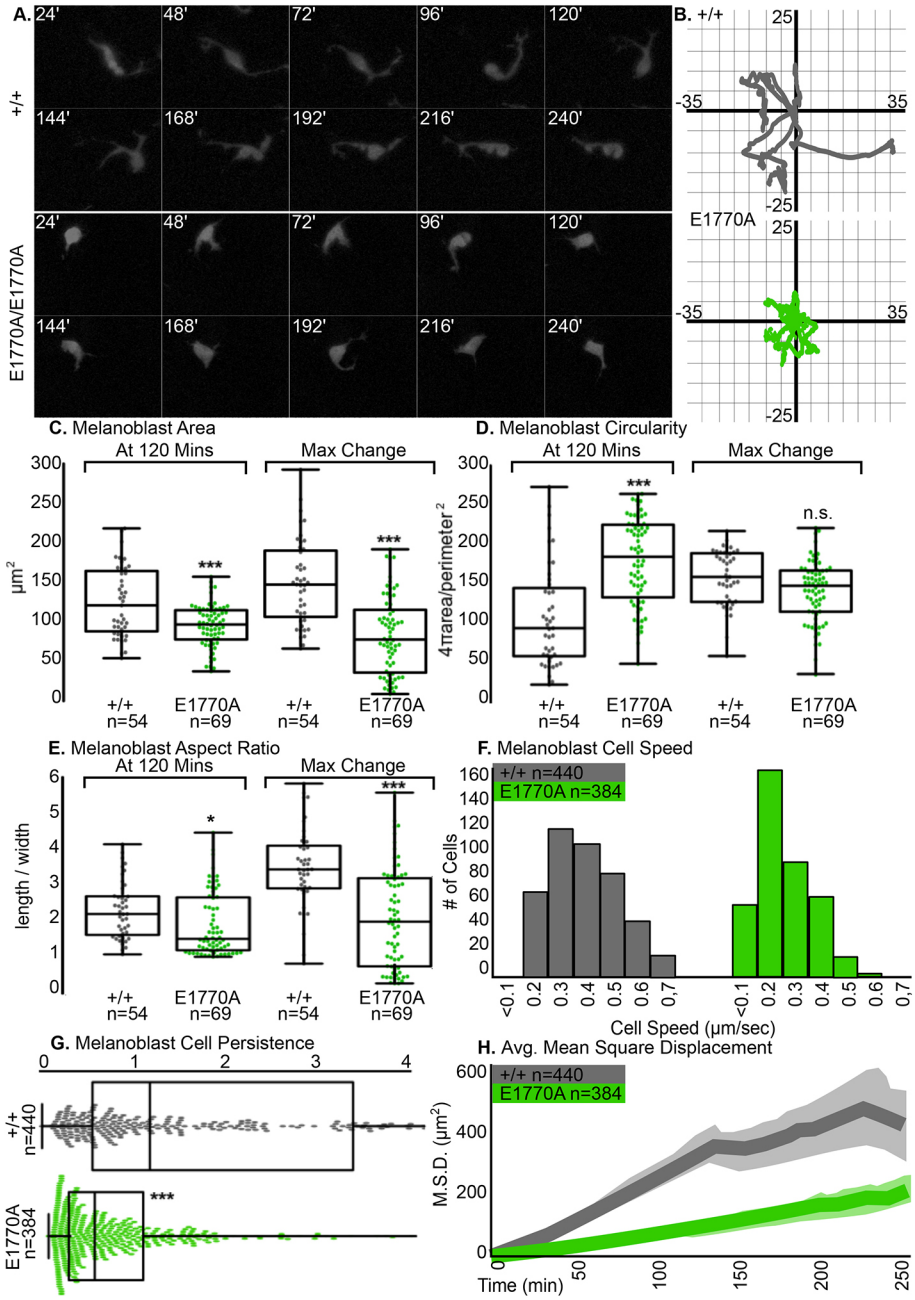


**Fig. 6. Loss of talin autoinhibition results in less dynamic melanoblasts *ex vivo*.** (A) Time series of single cells from a *Tln1*$^{+/+}$ or *Tln1*$^{E1770A/E1770A}$*::Mitf-Cre::Rosa26-floxed stop-TdTomato* E15.5 embryo trunk skin explant (Movies 3 and 4). (B) Cell trajectories from Movies 1 and 2. (C-E) Melanoblast areas (C), melanoblast circularities (D) and melanoblast aspect ratios (E) collected from five *Tln1*$^{+/+}$*::Mitf-Cre::Rosa26-floxed stop-TdTomato* and four *Tln1*$^{E1770A/E1770A}$*::Mitf-Cre::Rosa26-floxed stop-TdTomato ex vivo* movies. Cells were included that persisted in frame for the entire 4 h. Left charts represent shape measurements at 120 min into *ex vivo* movies. Right charts represent the max change in shape measurements (minimum value subtracted from maximum value) throughout an entire 4 h movie. (F) Cell speeds from *ex vivo* movies binned in groups ranging from <0.1 μm/s to 0.7 μm/s. *n*-values represent the number of cells. (G) Cell persistence, defined as the slope of the MSD over time, from *ex vivo* movies. Data points >0.05 not shown. *n*-values represent the number of cells. (H) The average MSD for 440 *Tln1*$^{+/+}$ cells is plotted over time (gray solid line), with the shaded region representing the 95% confidence interval at each time point. The average MSD for 384 *Tln1*$^{E1770A/E1770A}$ cells is plotted over time (green solid line), with the shaded region representing the 95% confidence interval at each time point. Box plots show minimum/maximum whiskers with box boundaries as Q1/Q3 and center line representing the median. ***$P \leq 0.001$, *$P \leq 0.05$ (Student's *t*-test). n.s., not significant.

First, we were able to quantify the cell shape dynamics over time, referred to as 'maximum changes in shape', for melanoblasts that were tracked throughout a 4 h timelapse. The observed changes in shape were consistently lower in mutants than in wild-type controls (Fig. 6C-E, right). Tomato-positive melanoblast migration speed, persistence and mean square displacement (MSD) were also measured (Fig. 6F-H). This analysis showed that, compared with Tomato-positive melanoblasts from *Tln1*$^{+/+}$ control mice, Tomato-positive melanoblasts from *Tln1*$^{E1770A/E1770A}$ mutants did in fact exhibit substantially slower migration speeds and, in some cases, they did not migrate at all. (Fig. 6F, Movies 2 and 4). Moreover, *Tln1*$^{E1770A/E1770A}$ mutants also showed reduced migration persistence and lower MSD over time (Fig. 6G,H).

The decreased ability of melanoblasts from *Tln1*$^{E1770A/E1770A}$ mutants to migrate was associated with short protrusions produced in reduced number, consistent with increased cell-ECM adhesion. Our analysis of movies from skin explants of *Tln1*$^{E1770A/E1770A}$ mice showed that melanoblasts produced fewer protrusions compared with wild-type controls, and that this was seen both at a single timepoint (at 120 min) or as a sum of all protrusive activity throughout the movie (Fig. 7A,B). These results were also in line with what we saw in autoinhibition-defective primary melanocytes (Fig. 4A). Many melanoblasts from *Tln1*$^{E1770A/E1770A}$ mutants never produced protrusions throughout the course of the movies (Fig. 7B, Movies 1-4), but when they did, those protrusion typically had similar lifetimes as those seen in wild-type controls (Fig. 7C). Though they lasted the same amount of time, protrusions from *Tln1*$^{E1770A/E1770A}$ melanoblasts were less complex, with less branching compared with wild-type controls (Fig. 7D), and were shorter in length (Fig. 7E). Wild-type melanoblasts were frequently seen to produce long protrusions that allowed the cell body to translocate over that protrusion, moving the cell large distances at a

Development (2020) 147, dev184234. doi:10.1242/dev.184234

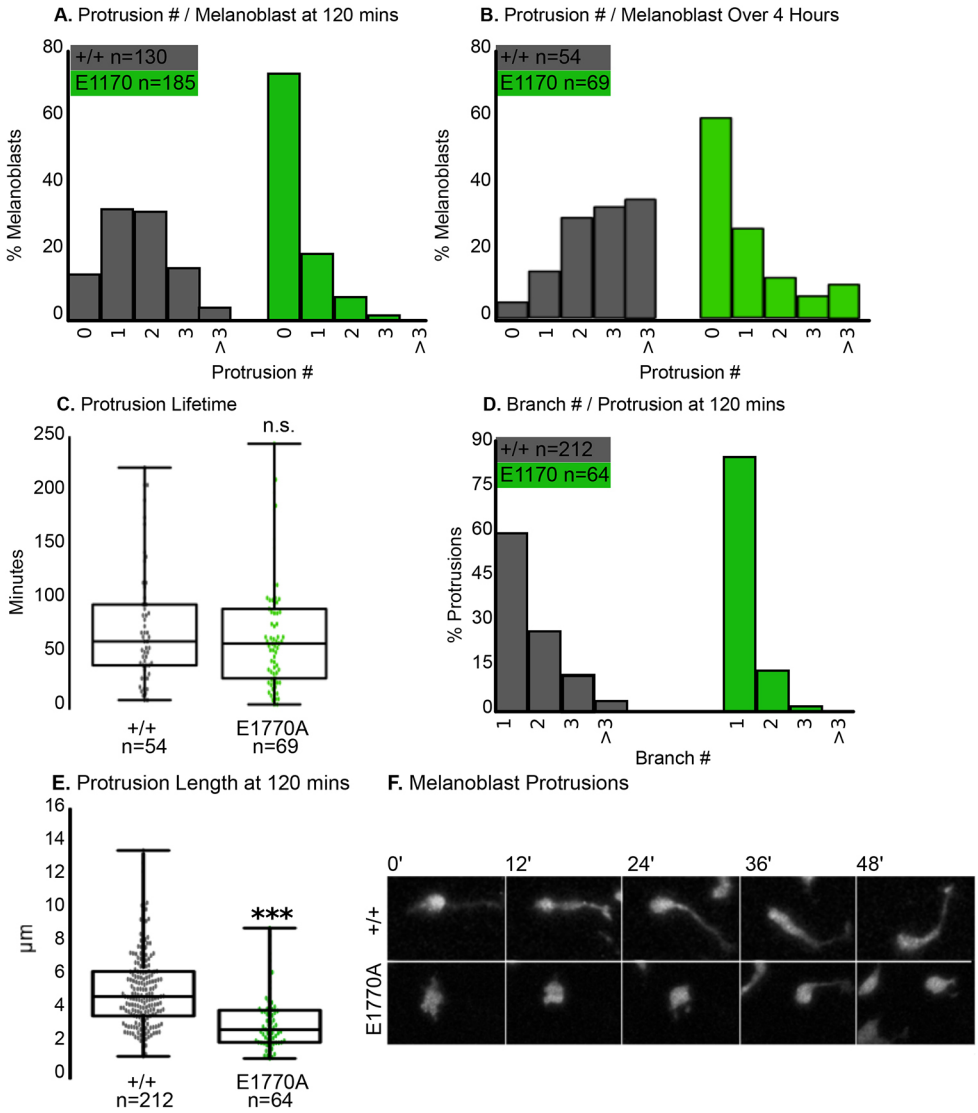


**Fig. 7. Loss of talin autoinhibition results in fewer, shorter protrusions *ex vivo*.** (A) Percentage of melanoblasts binned by number of protrusions. Protrusions per melanoblast were counted at 120 min into 4 h *ex vivo* movies. (B) Percentage of melanoblasts binned by the number of protrusions produced throughout entire 4 h *ex vivo* movies. (C) Protrusion lifetime from *ex vivo* movies. (D) Percentage of protrusions identified in A binned by number of branches. Branches were defined as protrusions not directly attached to the cell body. (E) Protrusion length of protrusions identified in A. (F) Representative time series of melanoblast protrusions from *ex vivo* movies. Box plots show minimum/maximum whiskers with box boundaries as Q1/Q3 and center line representing the median. ***$P \leq 0.001$ (Student's *t*-test). n.s., not significant.

time (Fig. 7F). Comparatively, melanoblasts lacking talin autoinhibition produce fewer short protrusions, allowing the cell body to translocate less frequently and over shorter distances (Fig. 7F). Taken together, our data show that cell migration efficiency is reduced in talin autoinhibition-defective melanoblasts.

### Integrins contribute to melanoblast migration

As the E1770A mutation in talin impinges on a regulatory mechanism that imparts an inhibitory effect on cell-ECM adhesion, it is expected to produce a gain-of-function phenotype. The phenotypes observed in melanoblasts and melanocytes both at the level of whole cells or individual FAs are consistent with previous results in fibroblasts that support such an interpretation (Haage et al., 2018). For this reason, it is possible that the melanoblast migration defects we observe in *Tln1*$^{E1770A/E1770A}$ mutant embryos reflects an ectopic gain-of-function phenotype rather than the endogenous role of integrin-mediated cell-ECM adhesion in this process. Melanocytes are known to express multiple integrin heterodimers including α3β1, α5β1, α6β1 and $\alpha_V$β3 that each have different ECM ligand binding partners and have a distinct temporal and spatial distribution (Hara et al., 1994; Morelli et al., 1993; Scott et al., 1992; Zambruno et al., 1993). Attachment of melanocytes to the substratum was reported to be primarily mediated by α6β1 integrins, whereas α3β1, α5β1 and $\alpha_V$β3 integrins were reported to mediate melanocyte dendrite outgrowth (Hara et al., 1994). However, to date, the contribution of the various integrin subunits to melanoblast migration has not been analyzed genetically. We chose to investigate the role of α6β1 integrin in melanoblasts by inducing a complete deletion of *Itga6* specifically in melanocytes using a Cre-loxP approach (De Arcangelis et al., 2017). A targeted cell-type specific knockout approach is necessary as the hemidesmosomal α6β4 integrin heterodimer is essential for skin development (Georges-Labouesse et al., 1996). We obtained a conditional α6 integrin floxed allele of *Itga6* (*Itga6*$^{fl/fl}$) that has previously been shown to completely eliminate its expression (De Arcangelis et al., 2017) and combined it with the neural crest-specific *Wnt1-Cre* transgene to produce *Itga6*$^{\Delta MEL/\Delta MEL}$ mice. The resulting *Itga6*$^{\Delta MEL/\Delta MEL}$ mice were viable and we did not observe any ventral white patches in any of our mice ($n$>10). The *Dct::lacZ* reporter was used to visualize and quantify melanoblasts in control *Itga6*$^{+/+}$ and *Itga6*$^{\Delta MEL/\Delta MEL}$ embryos (Fig. 8). No difference in the number of melanoblasts between control *Itga6*$^{+/+}$ and *Itga6*$^{\Delta MEL/\Delta MEL}$ mice was observed at E11.5 (Fig. 8A,B). Analysis of the average density of melanoblasts in E13.5 embryos by segmenting the skin into equal sized regions from dorsal to ventral showed similar distribution of melanoblasts in control *Itga6*$^{+/+}$ and *Itga6*$^{\Delta MEL/\Delta MEL}$ mice (Fig. 8C,D). However, in

Development (2020) 147, dev184234. doi:10.1242/dev.184234

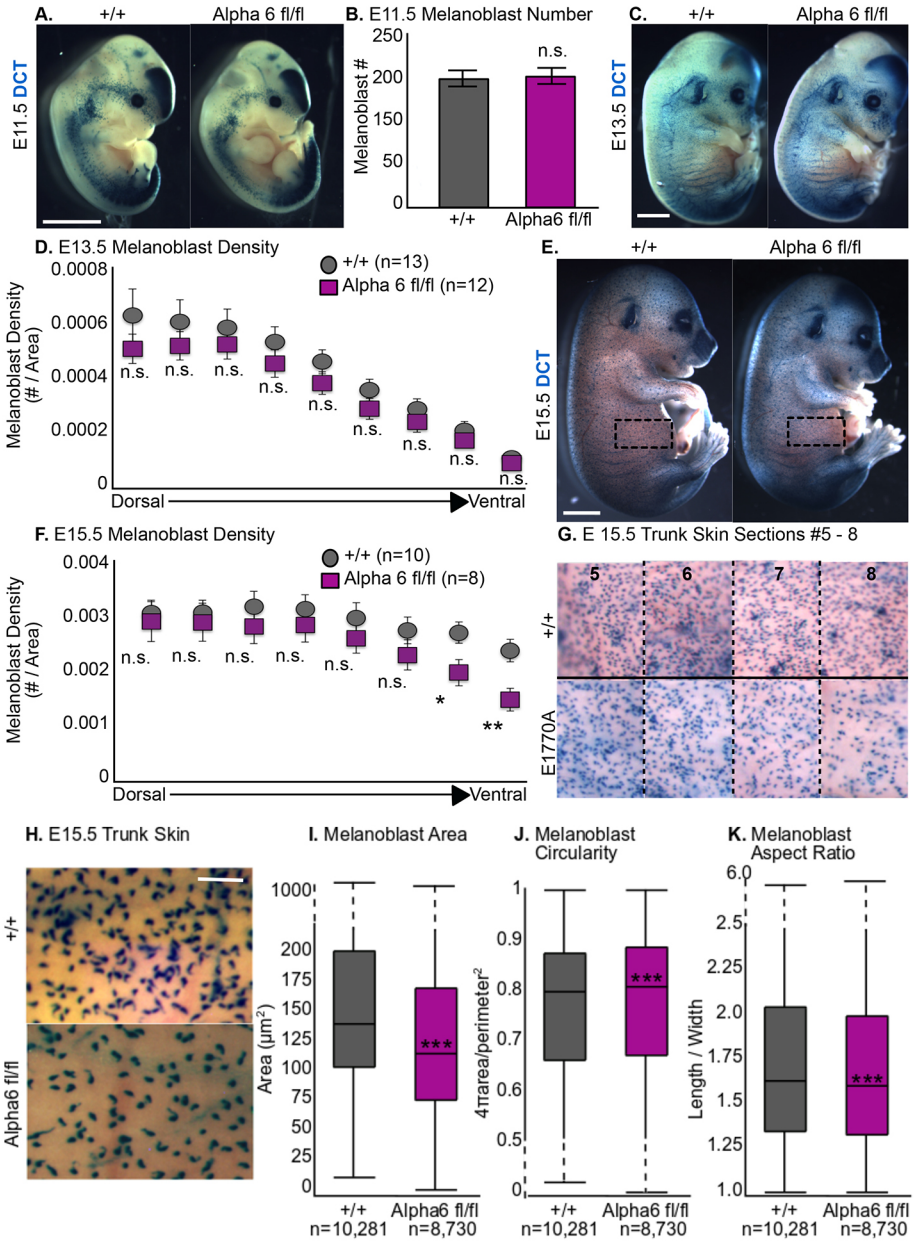


**Fig. 8. α6 Integrin contributes to melanoblast migration.** (A) Representative X-gal-stained E11.5 *Itga6*$^{+/+}$; *Dct::lacZ* and *Itga6*$^{\Delta MEL/\Delta MEL}$; *Dct::lacZ* embryos. (B) Mean number of melanoblasts counted in E11.5 embryos. (C) Representative X-gal-stained E13.5 *Itga6*$^{+/+}$; *Dct::lacZ* and *Itga6*$^{\Delta MEL/\Delta MEL}$; *Dct::lacZ* embryos. (D) Mean melanoblast density (number/segment area) from E13.5 embryo trunk segments. (E) Representative X-gal-stained E15.5 *Itga6*$^{+/+}$; *Dct::lacZ* and *Itga6*$^{\Delta MEL/\Delta MEL}$; *Dct::lacZ* embryos. Boxed areas indicate the position of quantified trunk regions. (F) Mean melanoblast density (number/segment area) from E15.5 embryo trunk segments. (G) Ventral-most segments of E15.5 embryos in E that were quantified. (H) High magnification representative images of the trunk of X-gal-stained E15.5 *Itga6*$^{+/+}$; *Dct::lacZ* and α6$^{\Delta MEL/\Delta MEL}$; *Dct::lacZ* embryos presented in E, showing individual melanoblasts. (I) Melanoblast areas from 13 *Itga6*$^{+/+}$; *Dct::lacZ* and 12 *Itga6*$^{\Delta MEL/\Delta MEL}$; *Dct::lacZ* E15.5 X-gal-stained embryos. (J) Melanoblast circularities from 13 *Itga6*$^{+/+}$; *Dct::lacZ* and 12 *Itga6*$^{\Delta MEL/\Delta MEL}$; *Dct::lacZ Itga6*$^{\Delta MEL}$ E15.5 X-gal-stained embryos. (K) Melanoblast aspect ratios from 13 *Itga6*$^{+/+}$; *Dct::lacZ* and 12 *Itga6*$^{\Delta MEL/\Delta MEL}$; *Dct::lacZ* E15.5 X-gal-stained embryos. Box plots show minimum/maximum whiskers with box boundaries as Q1/Q3 and center line representing the median. Error bars denote s.e.m. ***$P \leq 0.001$, **$P \leq 0.01$, *$P \leq 0.05$ (Student's *t*-test). n.s., not significant. Scale bars: 500 µm in A; 1 mm in C; 2 mm in E; 100 µm in H.

E15.5 embryos a small reduction was seen in the number of melanoblasts in the ventral-most segments in *Itga6*$^{\Delta MEL/\Delta MEL}$ mice, compared with control *Itga6*$^{+/+}$ mice (Fig. 8E-G). Next, we analyzed melanoblast cell shape in the context of the intact skin by taking high magnification images of melanoblasts labeled by *Dct::lacZ* from whole E15.5 embryos (Fig. 8H). Analysis of melanoblast shape was performed for control *Itga6*$^{+/+}$ and *Itga6*$^{\Delta MEL/\Delta MEL}$ embryos to measure their area, circularity and aspect ratio (see Materials and Methods). This analysis showed that, in the context of the intact skin, melanoblasts from *Itga6*$^{\Delta MEL/\Delta MEL}$ embryos exhibited features consistent with a reduced migratory phenotype; specifically, they were slightly rounder, occupied more area and had altered aspect ratio (Fig. 8I-K).These data suggest that α6β1 integrin-mediated cell-ECM adhesion contributes to melanoblast migration *in vivo*.

## DISCUSSION

The work presented here shows that the precise regulation of cell-ECM adhesion is essential for efficient dispersal of melanoblasts throughout the mouse skin. Moreover, our work suggests that talin autoinhibition plays a key role in regulating cell migration by controlling cell-ECM adhesion through the modulation of the number of active talin molecules in the cell. Increased talin activity because of loss of autoinhibition impacts the ability of melanoblasts to adopt a wild-type migratory phenotype. They are rounder and show less protrusive activity compared with controls. Moreover, cell-ECM adhesion is increased, as evidenced by FAs that show features consistent with more mature adhesions, as well as higher integrin activation and elevated attachment to the ECM. Collectively, these changes impact the ability of melanoblasts to migrate efficiently, which results in delayed movement within the skin and the absence of melanoblasts in the most ventral or distal areas of the body: the belly, toes and tail tip.

Our recent characterization of the role of talin autoinhibition in MEFs provides useful clues about the mechanisms that underlie the melanoblast migration defects we observed in autoinhibition mutants (Haage et al., 2018). In both MEFs and primary

Development (2020) 147, dev184234. doi:10.1242/dev.184234

melanocytes loss of talin autoinhibition gave rise to a similar array of phenotypes, both at the level of single FAs and the whole cell (Haage et al., 2018). As the phenotypes of talin autoinhibition-defective MEFs and primary melanocytes are similar in many respects we can speculate that this resemblance extends to other functional changes we described in MEFs. These phenotypes include reduced ability to impart traction force on the ECM and reduced adhesion complex dynamics. As the phenotypic changes induced by the talin autoinhibition mutation are not restricted to melanocytes, because they affect the whole animal, we cannot discount the possibility that the *in vivo* migration and pigmentation defects in talin autoinhibition mutants could also be due to changes in other tissues that contribute to migration. Nonetheless, the robust and diverse cellular phenotypes observed in cultured primary melanocytes from talin autoinhibition mutants are consistent with the interpretation that the impact of this mutation on cell-ECM adhesion in melanoblasts is, at the very least, a major contributor to their defective migration during embryogenesis.

One major phenotypic difference between melanocytes and MEFs in talin autoinhibition mutants is in the organization of the actin cytoskeleton. Compared with wild-type controls, MEFs from talin autoinhibition-defective mutants have increased actin dynamics and show a disorganized actin architecture (Haage et al., 2018). Surprisingly, these phenotypes were not observed in primary melanocytes cultured from talin autoinhibition-defective mutants. It has been shown that regulation of actin dynamics is key for melanoblast migration, and loss of fascin 1, which bundles and serves important roles in regulating actin, gives rise to pigmentation defects similar to those observed in talin autoinhibition mutants (Ma et al., 2013). In that light, it is unexpected that actin dynamics and organization are unaffected in talin autoinhibition-defective mutants. However, analysis on the role of CDC42 has illustrated that actin dynamics can be uncoupled from migration in melanoblasts, suggesting that various systems that generate motility in melanoblasts can function independently (Woodham et al., 2017). Taken together, these results suggest the existence of tissue-specific roles for talin autoinhibition in different cell types.

Integrins are involved in multiple migration processes that take place during mouse embryogenesis (Liu et al., 2009, 2011; Taylor-Weiner et al., 2015), many of which are essential for viability. Yet our talin autoinhibition-defective mice are viable. There are a few possible explanations for why this is the case. For example, other embryonic migration processes could have additional, redundant mechanisms that are absent in melanoblasts. Alternatively, melanoblast migration might be particularly sensitive to changes in cell motility because it involves a very long-range migration process. It could also be that other migration processes are partially disrupted, but in the absence of a clear visible readout, such as pigmentation defects, we have not yet detected these mild phenotypes. Future work will focus on careful quantifications of other migration processes in mouse embryogenesis that involve cell-ECM adhesion to determine whether these are also impinged upon by loss of talin autoinhibition.

It has been known for some time that multiple integrin heterodimers are expressed in melanoblasts. However, their role has been difficult to study for two main reasons. First, integrin heterodimers that have been detected in melanocytes are also involved in other important biological processes that disrupt embryogenesis at stages that precede melanoblast migration. For this reason, analyzing the specific roles integrins play in melanoblasts requires the availability of conditional alleles and appropriate Cre driver lines. Second, there can be substantial redundancy between integrin heterodimers and, consequently, loss of any one heterodimer will produce only weak phenotypes. For example, it is unlikely that we would have detected the subtle migration defects we observed following melanoblast-specific depletion of α6 integrin had we not specifically looked for such phenotypes using sensitive quantitative tools. In this regard, our results highlight the utility of using gain-of-function strategies exemplified by the talin autoinhibition mutant. Not only does such an approach circumvent the issue of redundant integrin function, but it also allows the detection of a range of phenotypes that might otherwise be obscured in loss-of-function integrin mutants owing to the presence of severe developmental disruptions.

## MATERIALS AND METHODS

### Mice

*Tln1*$^{E1770A}$ mice were generated by genOway on the C57BL/6J genetic background (previously described by Haage et al., 2018). Wnt1-cre mice were purchased from The Jackson Laboratory on the C57BL/6J background and genotyped per their protocol. These were then combined with α6$^{fl/fl}$ mice, a generous gift from Susanne M Clee from the University of British Columbia, Canada. The α6$^{fl/fl}$ mice have previously been described (De Arcangelis et al., 2017). *Dct::lacZ*, *Mitf-cre*, and *Rosa26-floxed stop-TdTomato* mice were supplied by Cathy Van Raamsdonk from the University of British Columbia (Alizadeh et al., 2008; Mackenzie et al., 1997; Madisen et al., 2010). All animals were housed at the Centre for Disease Modeling at the University of British Columbia using standard husbandry. The University of British Columbia Animal Care and Use Program approved all procedures. All protocols complied with the national Canadian Council on Animal Care guidelines for the ethical care and use of experimental animals.

### Methodology details

#### Skin histology

Skin from $n$>3 ventral and dorsal trunk regions was collected from 4-week-old mice of each genotype. The skin was trimmed by a razor blade, fixed in 4% paraformaldehyde (PFA) for 30 min, and then embedded and frozen at −80°C in optimal cutting temperature compound (OCT). Non-sequential 150 µm thickness sections were then taken of each sample using a Leica cryostat CM3050. Sections were subjected to a sodium citrate antigen retrieval, 0.05% Triton-X permeabilization, blocked with donkey serum and bovine serum albumin, and then stained with 1:200 TRP2 primary antibody (D-18, sc-10451, Santa Cruz Biotechnology) and 1:500 donkey anti-goat AlexaFluor 488 secondary antibody (705-545-003, Jackson ImmunoResearch). Sections were then mounted using Vectashield (Vector Laboratories) containing DAPI stain.

#### Western blot analysis

Protein samples were extracted using RIPA buffer containing complete protease inhibitor cocktail (Roche) from the neural crest of E8.5 mouse embryos, incubated at 4°C for 2 h and centrifuged at 12,000 rpm (17,000 ***g***) at 4°C for 20 min. After addition of SDS sample buffer, samples were heated at 70° for 10 min and were resolved using a 7% gel. Primary antibodies used were 1:200 anti-talin (YQ-16, Santa Cruz Biotechnology) and 1:1000 anti-β actin (A1978, Sigma-Aldrich). Secondary antibody used was 1:3000 anti-mouse IgG conjugated to HRP (1706516, Bio-Rad). Chemiluminescent substrate (Clarity Western ECL, Bio-Rad) was applied according to the manufacturer's instruction and blots were imaged using a western blot scanner with a 6 min exposure.

#### *lacZ* whole embryo stains

*Tln1*$^{E1770A/+}$::*Dct::lacZ* and α6$^{\Delta MEL/+}$::*Dct::lacZ* mice were set up in timed mating intercrosses. Litters were harvested at E11.5, E13.5 and E15.5 days. Wild-type littermates were used as controls. Embryos were fixed in fixing buffer (2% formaldehyde, 0.2% glutaraldehyde, 0.02% NP-40, 1 mM $MgCl_2$, 0.1 mg/ml sodium deoxycholate) for 1 h for E11.5 and E13.5 and 3 h for E15.5. They were then stained in X-gal buffer (1 mg/ml X-gal, 4 mM potassium ferrocyanide, 4 mM ferricyanide, 2 mM $MgCl_2$) overnight.

Development (2020) 147, dev184234. doi:10.1242/dev.184234

#### EdU proliferation stains

A Click-iT™ EdU Alexa Fluor™ 555 Imaging Kit (Thermo Fisher) was used per the manufacturer's instructions. Briefly, *Tln1*$^{E1770A/+}$ mice were set up in timed mating intercrosses. Wild-type littermates were used as controls. Pregnant mice were injected with 100 µl of 10 mM EdU per 10 g of mouse body weight either 4 h or 24 h before harvest of embryos at E15.5. Embryos were then fixed for 24 h in 4% PFA at 4°C and embedded in OCT. Non-sequential 20 µm thickness transverse sections of the embryo trunk were then taken. Sections were stained for EdU as per kit instructions and then stained for Dct as described above.

#### Basement membrane stains

*Tln1*$^{E1770A/+}$ mice were set up in timed mating intercrosses. Wild-type littermates were used as controls. E15.5 embryos were fixed for 24 h in 4% PFA at 4°C, and embedded in OCT. Non-sequential 20 µm thickness transverse sections of the embryo trunk were then taken. Sections were stained with 1:40 collagen IV primary antibody (EMD Millipore, AB769); and 1:800 donkey anti-rabbit AlexaFluor 488 secondary antibody (711-545-152, Jackson ImmunoResearch), as well as Dct as described above.

#### Primary melanocyte culture and immunofluorescence

Primary melanocytes were isolated from postnatal day (P)3 *Tln1*$^{+/+}$ and *Tln1*$^{E1770A/E1770A}$ neonatal mice as previously described. Primary cultures were treated with 150 µM G418 for 4 days on, 3 days off for 6 weeks before use in experiments as previously described in order to remove any fibroblast contamination (Sviderskaya et al., 1997; Woodham et al., 2017). This procedure was validated with Dct antibody staining before experiments were conducted for this manuscript. For immunofluorescence, primary melanocytes were allowed to spread on 0.1 mg/ml fibronectin-coated coverslips for 180 min. The cells were then stained as previously described (Haage et al., 2018). A coverslip spinning assay was used as previously described to determine relative adhesion strength (García et al., 1997; Haage et al., 2018).

#### Live *ex vivo* skin culture

Experimental conditions were adapted from Cetera et al. (2018) and Mort et al. (2010). Briefly, *Tln1*$^{+/+}$*::MITF-cre::Rosa26-Tom* and *Tln1*$^{E1770A/E1770A}$*::MITF-cre::Rosa26-Tom* E15.5 embryos were harvested and dissected to remove sections of the trunk skin complete with epidermis and dermis. The skin was then sandwiched so that the epidermis was in contact with a gas permeable Lumox membrane in a 35-mm dish (Sarstedt) and the dermis was in contact with a 1% agarose pad made with phenol-free DMEM supplemented with 10% fetal bovine serum. The sandwich was then overlaid with 1 ml phenol-free DMEM supplemented with 10% fetal bovine serum and weighted for imaging.

### Quantification and statistical analysis

#### Hair follicle counts

The number of Dct-positive cells were counted per hair follicle from multiple skin sections from $n>3$ mice per genotype.

#### *lacZ*-stained melanoblast migration analysis

Whole embryos were imaged using a Leica MS5 microscope equipped with a QImaging Micropublisher 5.0 RTV camera. For quantifying E11.5 embryos, the number of individual melanoblasts discernible per embryo were counted manually. For quantifying E13.5 and E15.5 embryos, the trunk region was defined as a rectangle from the spinal cord to the belly apex in between the two limb joints. This rectangle was then split into equal area segments, nine for E13.5 and eight for E15.5. Melanoblasts in each segment were then counted using an auto local threshold and analyzed particles in ImageJ. This number was then divided by the area of the segment to create a density measurement.

#### EdU proliferation analysis and Dct-stained melanoblast shape analysis

The number of Dct and EdU double-positive cells were counted from multiple sections from $n>3$ E15.5 embryos per genotype. This was then divided by the total number of Dct-positive cells found in these sections. Dct-positive cells from these sections were then also traced by hand in ImageJ to measure cell area, circularity and aspect ratio.

#### Primary melanocyte imaging and automated analysis

Fixed cell imaging and analysis was completed as previously described (Haage et al., 2018). Briefly, FAs, cell morphology and actin fibers were analyzed using custom MATLAB protocols. To quantify actin fibers specifically we adapted previously used methods from Cetera et al. (2014) to calculate a 2D Fourier transform across each cell in overlapping windows. Fibrousness is then based on the aspect ratio of this Fourier transform.

#### Skin imaging and analysis

Explants were imaged live at 37°C on an Olympus Fluoview (FV1000) inverted confocal microscope. Stacks were taken every 2 min. The resulting movies were then analyzed using the ADAPT plug-in for ImageJ (Barry et al., 2015). This provided the automated analysis of migration trajectories, speed, MSD and cell morphologies. Cell persistence was then calculated as the slope of MSD plotted over time per cell. Protrusion measurements were completed by hand. Protrusions were counted that originated from the cell body, branches were counted that originated from pre-existing protrusions.

#### Acknowledgements

The authors acknowledge the Clee lab at the University of British Columbia for the *Itga6*$^{fl/fl}$ mice. The authors also thank the following undergraduate students for help with the preliminary analysis of the *Dct::lacZ* stained embryos: Tanja Schuster, Chae Shin and Yolanda Rao.

#### Competing interests

The authors declare no competing or financial interests.

#### Author contributions

Conceptualization: A.H., K.W., K.G., G.T.; Methodology: A.H., K.W., A.B.; Software: A.H., K.G.; Validation: A.H.; Formal analysis: A.H., K.W., C.M.; Investigation: A.H., K.W., W.D., B.V., C.M.; Resources: A.H., K.W., C.M., A.B., L.L., C.D.V.R; Data curation: A.H.; Writing - original draft: A.H., G.T.; Writing - review & editing: A.H., K.W., C.M., K.G., A.B., G.T.; Visualization: A.H.; Supervision: A.H., L.L., C.D.V.R., G.T.; Project administration: A.H., G.T.; Funding acquisition: A.H., L.L., C.D.V.R., G.T.

#### Funding

This study was supported by Canadian Institutes of Health Research Operating Grants to G.T. (MOP-285391) and L.L. (MOP-119357), as well as a Natural Sciences and Engineering Research Council of Canada Discovery Grant to L.L. (386979-12).

#### Supplementary information

Supplementary information available online at
https://dev.biologists.org/lookup/doi/10.1242/dev.184234.supplemental

#### Peer review history

The peer review history is available online at
https://dev.biologists.org/lookup/doi/10.1242/dev.184234.reviewer-comments.pdf

#### References

**Adameyko, I., Lallemend, F., Aquino, J. B., Pereira, J. A., Topilko, P., Müller, T., Fritz, N., Beljajeva, A., Mochii, M., Liste, I. et al.** (2009). Schwann cell precursors from nerve innervation are a cellular origin of melanocytes in skin. *Cell* **139**, 366-379. doi:10.1016/j.cell.2009.07.049

**Alizadeh, A., Fitch, K. R., Niswender, C. M., McKnight, G. S. and Barsh, G. S.** (2008). Melanocyte-lineage expression of Cre recombinase using Mitf regulatory elements. *Pigment Cell Melanoma Res.* **21**, 63-69. doi:10.1111/j.1755-148X.2007.00425.x

**Barry, D. J., Durkin, C. H., Abella, J. V. and Way, M.** (2015). Open source software for quantification of cell migration, protrusions, and fluorescence intensities. *J. Cell Biol.* **209**, 163-180. doi:10.1083/jcb.201501081

**Bazzoni, G., Shih, D.-T., Buck, C. A. and Hemler, M. E.** (1995). Monoclonal antibody 9EG7 defines a novel beta 1 integrin epitope induced by soluble ligand and manganese, but inhibited by calcium. *J. Biol. Chem.* **270**, 25570-25577. doi:10.1074/jbc.270.43.25570

**Beauvais-Jouneau, A., Pla, P., Bernex, F., Dufour, S., Salamero, J., Fässler, R., Panthier, J.-J., Thiery, J. P. and Larue, L.** (1999). A novel model to study the dorsolateral migration of melanoblasts. *Mech. Dev.* **89**, 3-14. doi:10.1016/S0925-4773(99)00191-4

**Bronner, M. E.** (2012). Formation and migration of neural crest cells in the vertebrate embryo. *Histochem. Cell Biol.* **138**, 179-186. doi:10.1007/s00418-012-0999-z
**Calderwood, D. A.** (2004). Integrin activation. *J. Cell Sci.* **117**, 657-666. doi:10.1242/jcs.01014
**Cetera, M., Ramirez-San Juan, G. R., Oakes, P. W., Lewellyn, L., Fairchild, M. J., Tanentzapf, G., Gardel, M. L. and Horne-Badovinac, S.** (2014). Epithelial rotation promotes the global alignment of contractile actin bundles during Drosophila egg chamber elongation. *Nat. Commun.* **5**, 5511. doi:10.1038/ncomms6511
**Cetera, M., Leybova, L., Joyce, B. and Devenport, D.** (2018). Counter-rotational cell flows drive morphological and cell fate asymmetries in mammalian hair follicles. *Nat. Cell Biol.* **20**, 541-552. doi:10.1038/s41556-018-0082-7
**De Arcangelis, A., Hamade, H., Alpy, F., Normand, S., Bruyère, E., Lefebvre, O., Méchine-Neuville, A., Siebert, S., Pfister, V., Lepage, P. et al.** (2017). Hemidesmosome integrity protects the colon against colitis and colorectal cancer. *Gut* **66**, 1748-1760. doi:10.1136/gutjnl-2015-310847
**Dedden, D., Schumacher, S., Kelley, C. F., Zacharias, M., Biertümpfel, C., Fässler, R. and Mizuno, N.** (2019). The architecture of talin1 reveals an autoinhibition mechanism. *Cell* **179**, 120-131.e13. doi:10.1016/j.cell.2019.08.034
**Devreotes, P. and Horwitz, A. R.** (2015). Signaling networks that regulate cell migration. *Cold Spring Harb. Perspect. Biol.* **7**, a005959. doi:10.1101/cshperspect.a005959
**Ellis, S. J., Goult, B. T., Fairchild, M. J., Harris, N. J., Long, J., Lobo, P., Czerniecki, S., Van Petegem, F., Schöck, F., Peifer, M. et al.** (2013). Talin autoinhibition is required for morphogenesis. *Curr. Biol. CB* **23**, 1825-1833. doi:10.1016/j.cub.2013.07.054
**García, A. J., Ducheyne, P. and Boettiger, D.** (1997). Quantification of cell adhesion using a spinning disc device and application to surface-reactive materials. *Biomaterials* **18**, 1091-1098. doi:10.1016/S0142-9612(97)00042-2
**Geiger, B. and Yamada, K. M.** (2011). Molecular architecture and function of matrix adhesions. *Cold Spring Harb. Perspect. Biol.* **3**, a005033. doi:10.1101/cshperspect.a005033
**Georges-Labouesse, E., Messaddeq, N., Yehia, G., Cadalbert, L., Dierich, A. and Le Meur, M.** (1996). Absence of integrin α6 leads to epidermolysis bullosa and neonatal death in mice. *Nat. Genet.* **13**, 370-373. doi:10.1038/ng0796-370
**Ginsberg, M. H.** (2014). Integrin activation. *BMB Rep.* **47**, 655-659. doi:10.5483/BMBRep.2014.47.12.241
**Goult, B. T., Bate, N., Anthis, N. J., Wegener, K. L., Gingras, A. R., Patel, B., Barsukov, I. L., Campbell, I. D., Roberts, G. C. K. and Critchley, D. R.** (2009). The structure of an interdomain complex that regulates talin activity. *J. Biol. Chem.* **284**, 15097-15106. doi:10.1074/jbc.M900078200
**Haage, A., Goodwin, K., Whitewood, A., Camp, D., Bogutz, A., Turner, C. T., Granville, D. J., Lefebvre, L., Plotnikov, S., Goult, B. T. et al.** (2018). Talin autoinhibition regulates cell-ECM adhesion dynamics and wound healing in vivo. *Cell Rep.* **25**, 2401-2416.e5. doi:10.1016/j.celrep.2018.10.098
**Hara, M., Yaar, M., Tang, A., Eller, M. S., Reenstra, W. and Gilchrest, B. A.** (1994). Role of integrins in melanocyte attachment and dendricity. *J. Cell Sci.* **107**, 2739-2748.
**Hirobe, T.** (2011). How are proliferation and differentiation of melanocytes regulated? *Pigment Cell Melanoma Res.* **24**, 462-478. doi:10.1111/j.1755-148X.2011.00845.x
**Hornberger, L. K., Singhroy, S., Cavalle-Garrido, T., Tsang, W., Keeley, F. and Rabinovitch, M.** (2000). Synthesis of extracellular matrix and adhesion through β1 integrins are critical for fetal ventricular myocyte proliferation. *Circ. Res.* **87**, 508-515. doi:10.1161/01.RES.87.6.508
**Huang, J. L.-Y., Urtatiz, O. and Raamsdonk, C. D. V.** (2015). Oncogenic G protein GNAQ induces uveal melanoma and intravasation in mice. *Cancer Res.* **75**, 3384-3397. doi:10.1158/0008-5472.CAN-14-3229
**Huttenlocher, A. and Horwitz, A. R.** (2011). Integrins in cell migration. *Cold Spring Harb. Perspect. Biol.* **3**, a005074. doi:10.1101/cshperspect.a005074
**Jordan, S. A. and Jackson, I. J.** (2000). MGF (KIT Ligand) is a chemokinetic factor for melanoblast migration into hair follicles. *Dev. Biol.* **225**, 424-436. doi:10.1006/dbio.2000.9856
**Jülich, D., Cobb, G., Melo, A. M., McMillen, P., Lawton, A. K., Mochrie, S. G. J., Rhoades, E. and Holley, S. A.** (2015). Cross-scale integrin regulation organizes ECM and tissue topology. *Dev. Cell* **34**, 33-44. doi:10.1016/j.devcel.2015.05.005
**Klapholz, B. and Brown, N. H.** (2017). Talin – the master of integrin adhesions. *J. Cell Sci.* **130**, 2435-2446. doi:10.1242/jcs.190991
**Lee, H.-S., Anekal, P., Lim, C. J., Liu, C.-C. and Ginsberg, M. H.** (2013). Two modes of integrin activation form a binary molecular switch in adhesion maturation. *Mol. Biol. Cell* **24**, 1354-1362. doi:10.1091/mbc.e12-09-0695
**Li, A., Ma, Y., Yu, X., Mort, R. L., Lindsay, C., Stevenson, D., Strathdee, D., Insall, R. H., Chernoff, J., Snapper, S. B. et al.** (2011). Rac1 drives melanoblast organization during mouse development by orchestrating pseudopod-driven motility and cell cycle progression. *Dev. Cell* **21**, 722-734. doi:10.1016/j.devcel.2011.07.008
**Lindsay, C. R., Lawn, S., Campbell, A. D., Faller, W. J., Rambow, F., Mort, R. L., Timpson, P., Li, A., Cammareri, P., Ridgway, R. A. et al.** (2011). P-Rex1 is required for efficient melanoblast migration and melanoma metastasis. *Nat. Commun.* **2**, 555. doi:10.1038/ncomms1560
**Liu, J., He, X., Corbett, S. A., Lowry, S. F., Graham, A. M., Fässler, R. and Li, S.** (2009). Integrins are required for the differentiation of visceral endoderm. *J. Cell Sci.* **122**, 233-242. doi:10.1242/jcs.037663
**Liu, J., He, X., Qi, Y., Tian, X., Monkley, S. J., Critchley, D. R., Corbett, S. A., Lowry, S. F., Graham, A. M. and Li, S.** (2011). Talin1 regulates integrin turnover to promote embryonic epithelial morphogenesis. *Mol. Cell. Biol.* **31**, 3366-3377. doi:10.1128/MCB.01403-10
**Loganathan, R., Rongish, B. J., Smith, C. M., Filla, M. B., Czirok, A., Bénazéraf, B. and Little, C. D.** (2016). Extracellular matrix motion and early morphogenesis. *Dev. Camb. Engl.* **143**, 2056-2065. doi:10.1242/dev.127886
**Ma, Y., Li, A., Faller, W. J., Libertini, S., Fiorito, F., Gillespie, D. A., Sansom, O. J., Yamashiro, S. and Machesky, L. M.** (2013). Fascin 1 is transiently expressed in mouse melanoblasts during development and promotes migration and proliferation. *Dev. Camb. Engl.* **140**, 2203-2211. doi:10.1242/dev.089789
**Mackenzie, M. A. F., Jordan, S. A., Budd, P. S. and Jackson, I. J.** (1997). Activation of the receptor tyrosine kinase Kit is required for the proliferation of melanoblasts in the mouse embryo. *Dev. Biol.* **192**, 99-107. doi:10.1006/dbio.1997.8738
**Madisen, L., Zwingman, T. A., Sunkin, S. M., Oh, S. W., Zariwala, H. A., Gu, H., Ng, L. L., Palmiter, R. D., Hawrylycz, M. J., Jones, A. R. et al.** (2010). A robust and high-throughput Cre reporting and characterization system for the whole mouse brain. *Nat. Neurosci.* **13**, 133-140. doi:10.1038/nn.2467
**Mayer, T. C.** (1973). The migratory pathway of neural crest cells into the skin of mouse embryos. *Dev. Biol.* **34**, 39-46. doi:10.1016/0012-1606(73)90337-0
**Mayor, R. and Theveneau, E.** (2013). The neural crest. *Development* **140**, 2247-2251. doi:10.1242/dev.091751
**Morelli, J. G., Yohn, J. J., Zekman, T. and Norris, D. A.** (1993). Melanocyte movement in vitro: role of matrix proteins and integrin receptors. *J. Invest. Dermatol.* **101**, 605-608. doi:10.1111/1523-1747.ep12366064
**Mort, R. L., Hay, L. and Jackson, I. J.** (2010). Ex vivo live imaging of melanoblast migration in embryonic mouse skin. *Pigment Cell Melanoma Res.* **23**, 299-301. doi:10.1111/j.1755-148X.2010.00669.x
**Mort, R. L., Jackson, I. J. and Patton, E. E.** (2015). The melanocyte lineage in development and disease. *Development* **142**, 620-632. doi:10.1242/dev.106567
**Parsons, J. T., Horwitz, A. R. and Schwartz, M. A.** (2010). Cell adhesion: integrating cytoskeletal dynamics and cellular tension. *Nat. Rev. Mol. Cell Biol.* **11**, 633-643. doi:10.1038/nrm2957
**Perris, R. and Perissinotto, D.** (2000). Role of the extracellular matrix during neural crest cell migration. *Mech. Dev.* **95**, 3-21. doi:10.1016/S0925-4773(00)00365-8
**Pines, M., Fairchild, M. J. and Tanentzapf, G.** (2011). Distinct regulatory mechanisms control integrin adhesive processes during tissue morphogenesis. *Dev. Dyn.* **240**, 36-51. doi:10.1002/dvdy.22488
**Schwartz, M. A.** (2010). Integrins and extracellular matrix in mechanotransduction. *Cold Spring Harb. Perspect. Biol.* **2**, a005066. doi:10.1101/cshperspect.a005066
**Schwartz, M. A. and Assoian, R. K.** (2001). Integrins and cell proliferation: regulation of cyclin-dependent kinases via cytoplasmic signaling pathways. *J. Cell Sci.* **114**, 2553-2560.
**Scott, G., Ryan, D. H. and McCarthy, J. B.** (1992). Molecular mechanisms of human melanocyte attachment to fibronectin. *J. Invest. Dermatol.* **99**, 787-794. doi:10.1111/1523-1747.ep12614749
**Scott, G., Ewing, J., Ryan, D. and Abboud, C.** (1994). Stem cell factor regulates human melanocyte-matrix interactions. *Pigment Cell Res.* **7**, 44-51. doi:10.1111/j.1600-0749.1994.tb00017.x
**Sviderskaya, E. V., Bennett, D. C., Ho, L., Bailin, T., Lee, S.-T. and Spritz, R. A.** (1997). Complementation of hypopigmentation in p-Mutant (Pink-Eyed Dilution) mouse melanocytes by normal human P cDNA, and defective complementation by OCA2 mutant sequences. *J. Invest. Dermatol.* **108**, 30-34. doi:10.1111/1523-1747.ep12285621
**Tadokoro, S., Shattil, S. J., Eto, K., Tai, V., Liddington, R. C., de Pereda, J. M., Ginsberg, M. H. and Calderwood, D. A.** (2003). Talin binding to integrin beta tails: a final common step in integrin activation. *Science* **302**, 103-106. doi:10.1126/science.1086652
**Taylor-Weiner, H., Ravi, N. and Engler, A. J.** (2015). Traction forces mediated by integrin signaling are necessary for definitive endoderm specification. *J. Cell Sci.* **128**, 1961-1968. doi:10.1242/jcs.166157
**Thomas, A. J. and Erickson, C. A.** (2008). The making of a melanocyte: the specification of melanoblasts from the neural crest. *Pigment Cell Melanoma Res.* **21**, 598-610. doi:10.1111/j.1755-148X.2008.00506.x
**Tokuo, H., Bhawan, J. and Coluccio, L. M.** (2018). Myosin X is required for efficient melanoblast migration and melanoma initiation and metastasis. *Sci. Rep.* **8**, 10449. doi:10.1038/s41598-018-28717-y
**Tsatmali, M., Ancans, J. and Thody, A. J.** (2002). Melanocyte function and its control by melanocortin peptides. *J. Histochem. Cytochem. Off. J. Histochem. Soc.* **50**, 125-133. doi:10.1177/002215540205000201
**Wolfenson, H., Lubelski, A., Regev, T., Klafter, J., Henis, Y. I. and Geiger, B.** (2009). A role for the juxtamembrane cytoplasm in the molecular dynamics of focal adhesions. *PLoS ONE* **4**, e4304. doi:10.1371/journal.pone.0004304
**Woodham, E. F., Paul, N. R., Tyrrell, B., Spence, H. J., Swaminathan, K., Scribner, M. R., Giampazolias, E., Hedley, A., Clark, W., Kage, F. et al.** (2017). Coordination by Cdc42 of actin, contractility, and adhesion for melanoblast movement in mouse skin. *Curr. Biol. CB* **27**, 624-637. doi:10.1016/j.cub.2017.01.033

Development (2020) 147, dev184234. doi:10.1242/dev.184234

**Wozniak, M. A., Modzelewska, K., Kwong, L. and Keely, P. J.** (2004). Focal adhesion regulation of cell behavior. *Biochim. Biophys. Acta BBA Mol. Cell Res.* **1692**, 103-119. doi:10.1016/j.bbamcr.2004.04.007

**Zambruno, G., Marchisio, P. C., Melchiori, A., Bondanza, S., Cancedda, R. and De Luca, M.** (1993). Expression of integrin receptors and their role in adhesion, spreading and migration of normal human melanocytes. *J. Cell Sci.* **105**, 179-190.

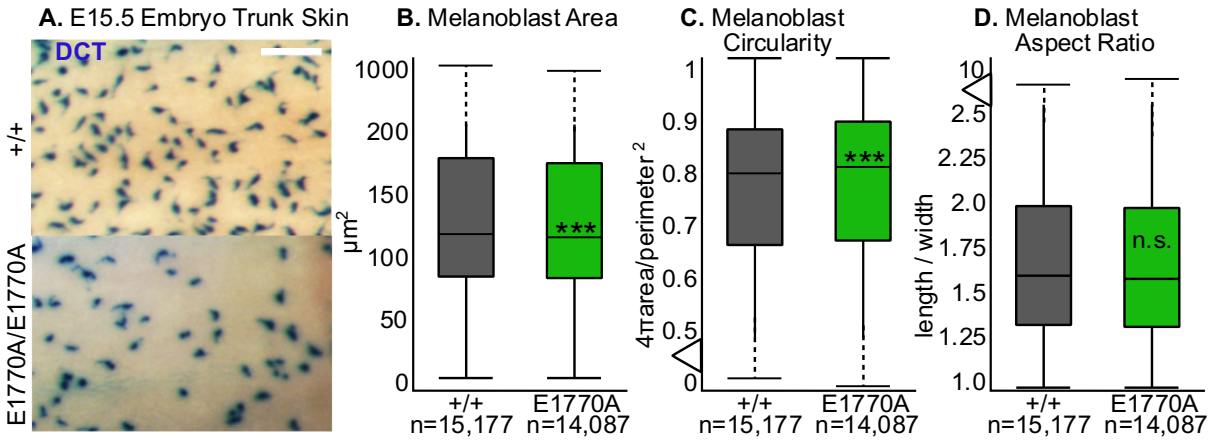


**Figure S1: Melanoblasts Lacking Talin Autoinhibition Exhibit Changes in Cell Shape in Intact Embryo Skin**

(A) High magnification representative images of the trunk of X-gal stained E15.5 *Tln1*$^{+/+}$; Dct::LacZ and *Tln1*$^{E1770A/E1770A}$; Dct::LacZ embryos, presented in Figure 2H, showing individual melanoblasts. (B-D) 16 *Tln1*$^{+/+}$; Dct::LacZ and 13 *Tln1*$^{E1770A/E1770A}$; Dct::LacZ E15.5 embryos were stained with X-gal to measure. Scale bar 100 µm (B) Melanoblast area, (C) Melanoblast circularities, and (D) Melanoblast aspect ratios. Significance was determined with student t-test; $^{***}p \leq 0.001$, $^{**}p \leq 0.01$, and $^{*}p \leq 0.05$.

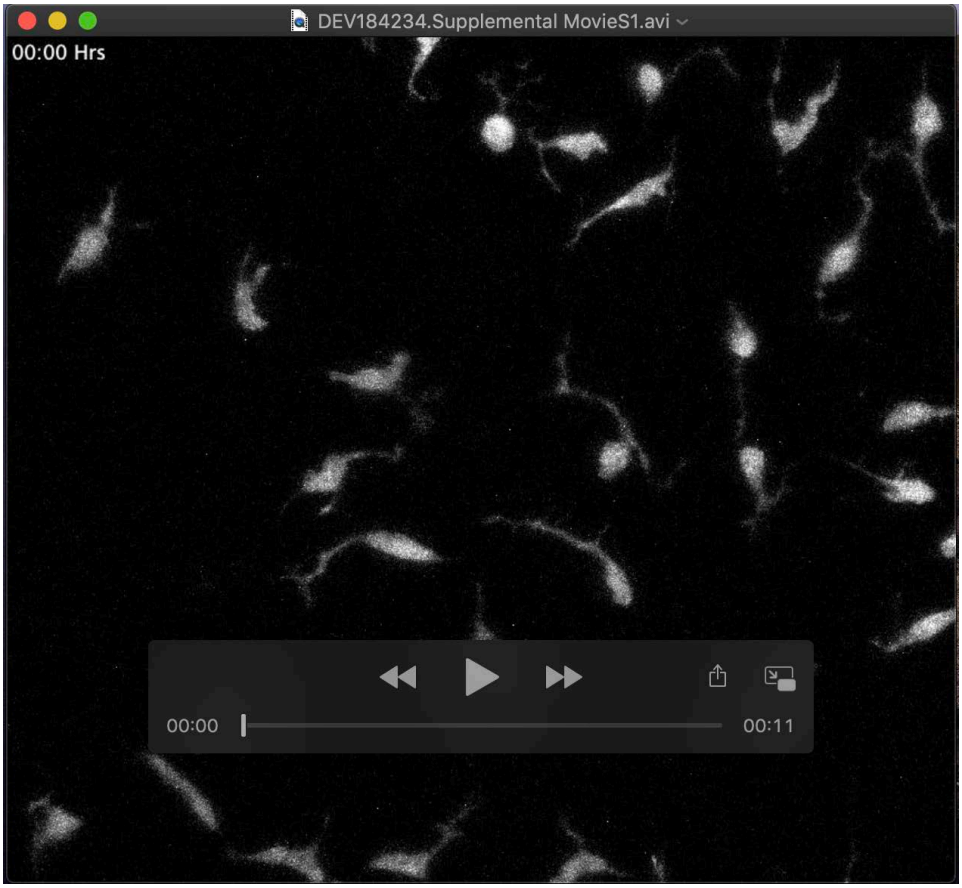


**Movie 1: Wildtype Melanoblasts Migrate in E15.5 Trunk Skin Explants, Related to Figure 6**

Trunk skin isolated from a *Tln1*$^{+/+}$::*Mitf-Cre*:: *Rosa26-floxed stop-TdTomato* embryo was cultured ex vivo and imaged every 2 minutes for 3 hours. Tracks of each cell are presented in Figure 6B. The movie plays at 7 frames per second.


**Movie 2: Talin Autoinhibition Defective Melanoblasts Migrate Less Efficiently, Related to Figure 6**

Trunk skin isolated from a *Tln1*$^{E1770A/E1770A}$::*Mitf-Cre*:: *Rosa26-floxed stop-TdTomato* embryo was cultured ex vivo and imaged every 2 minutes for 3 hours. Tracks of each cell are presented in Figure 6B. The movie plays at 7 frames per second.


**Movie 3: Single Cell Wildtype Melanoblast Migration, Related to Figure 6**

A single cell is focused on from trunk skin isolated from a *Tln1*$^{+/+}$::*Mitf-Cre*:: *Rosa26-floxed stop-TdTomato* embryo that was cultured ex vivo and imaged every 2 minutes for 4 hours.

Stills of this cell are presented over time in Figure 6A. The movie plays at 7 frames per second.

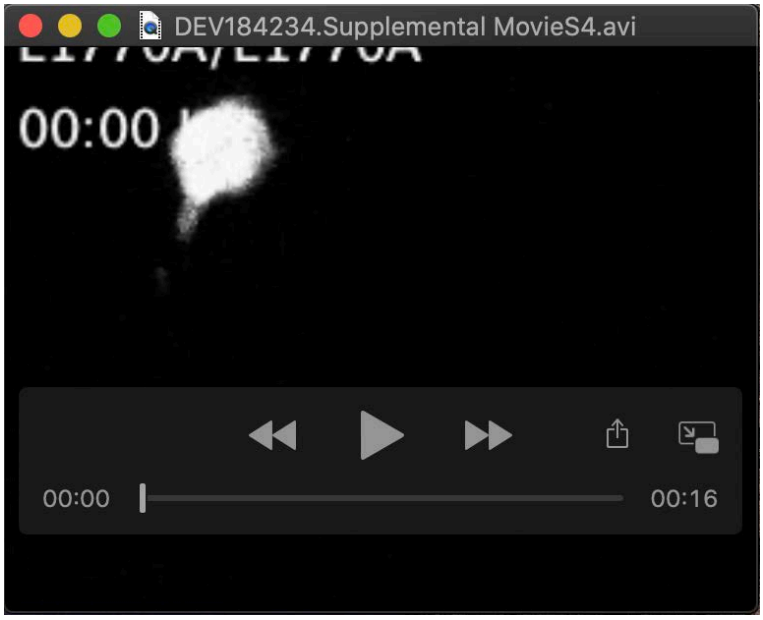


**Movie 4: Single Cell Talin Autoinhibition Defective Melanoblast Migration, Related to Figure 6**

A single cell is focused on from trunk skin isolated from a *Tln1*$^{E1770A/E1770A}$::*Mitf-Cre*::*Rosa26-floxed stop-TdTomato* embryo that was cultured ex vivo and imaged every 2 minutes for 4 hours. Stills of this cell are presented over time in Figure 6A. The movie plays at 7 frames per second.